Ψ_k **Scientific Highlight Of The Month**

No. 123 **June 2014**

Atomistic Spin Dynamics and Surface Magnons

Corina Etz[1], Lars Bergqvist[2], Anders Bergman[1], Andrea Taroni[1] and Olle Eriksson[1]

1) Department of Physics and Astronomy, Uppsala University, Box 516, 751 20 Uppsala, Sweden

2) KTH Royal Institute of Technology, Dept. of Materials and Nano Physics, Electrum 229, SE-164 40 Kista, Sweden

Abstract

Atomistic spin dynamics simulations has evolved to become a powerful and versatile tool for simulating dynamic properties in magnetic materials. It has a wide range of applications, for instance switching of magnetic states in bulk and nano magnets, dynamics of topological magnets like skyrmions and vortices and domain wall motion. In this review, we focus on calculations of spin wave excitations in low dimensional magnets and the effect on relativistic and temperature effects in such structures and compare the results with experimental values. In general, we find good agreement. For material specific studies, the atomistic spin dynamics is combined with electronic structure calculations within the density functional theory from which the required parameters are calculated, such as magnetic exchange interactions, anisotropy and Dzyaloshinskii-Moriya vectors.

1 Introduction

Establishing an understanding of materials invariably involves performing measurements of their properties. This gives information about the interactions of the material and the properties that result from these interactions. This applies e.g. to electron and heat conductivity, superconductivity, magnetism and structural properties. When it comes to crystal structures they are typically identified using x-ray diffraction[1], neutron scattering[2] or x-ray absorption fine structure (XAFS)[3]. For surfaces, low-energy electron diffraction (LEED) gives information about the atomic arrangement[4] and in an extension, the nature of the chemical interactions that favour a particular structure.

Probing magnetic structures and magnetic excitations is most frequently done with neutron scattering experiments, both in the elastic and inelastic mode[2]. Elastic neutron scattering experiments are important in that they give information about the magnetic ground state structure, e.g. a ferromagnetic, antiferromagnetic or non-collinear arrangement of the atomic spins[5]. Inelastic measurements probe both energy and momentum transfer and have the capability to map out the excitation spectrum of the material, i.e. the magnon dispersion relationship. Such measurements are important since the excitation spectrum reflects the strength of the interatomic

exchange parameters as well as the magnetic anisotropy constant and possibly the values of the Dzyaloshinskii-Moryia interaction. It was for the power of this experimental technique that the Nobel prize in physics was awarded to Brockhouse and Shull in 1994, with the motivation: *for pioneering contributions to the development of neutron scattering techniques for studies of condensed matter*. It is of relevance for this review to note that in these experiments, the differential cross section determines if a magnetic excitation can be observed [2].

For low dimensional systems and nano-magnets, neutron scattering experiments have not shown to be as useful as for bulk materials, since rather large samples have to be used in these experiments. Hence it was for a long time only possible to measure magnetic excitations of the bulk, while magnons of surfaces and thin films were eluding experimental investigations. This was the situation until the work of Ref.[6], where it was shown that spin-polarized EELS (SPEELS) can detect surface and interface magnons. Several intriguing results were found in these works, e.g. that the magnon dispersion of a monolayer of Fe on W(110) has a much softer magnon curve[7] compared to bulk Fe, and to early theories[8]. The possibility to experimentally detect excitations of buried interfaces was also shown to be possible[9]. In all these experimental works it was found that only the low-lying acoustic magnon mode had significant intensity in the experiments, a seemingly intriguing fact since optical modes should be possible from the experimental geometry, and they were even suggested from the theory of Ref.[9]. An explanation was proposed[10], that relates the SPEELS data to the differential cross section and dynamic structure factor, something we will return to later on in this review.

In parallel to the development of novel experimental methods there has been development also on the theory side, where in particular atomistic spin-dynamics (ASD), that couple electronic structure theory[11] to the equation of motion of atomistic spins, has proven particularly successful[12, 13, 14, 15]. There have by now been several publications of softwares that solve the atomistic spin-dynamics equation.

Theories based on ASD have been successful in describing many recent experiments of the magnetisation dynamics, for instance magnon dispersions of surfaces[10, 16, 17], all-thermal switching of Fe-Gd alloys[18] and thermal domain-wall motion[19]. This highlight is focused on the ASD method, and how it reproduces experimental magnon dispersions, in particular for low dimensional systems. Here, we will present results obtained by employing ASD, with other theories, e.g. frozen magnon calculations or dynamical susceptibility calculations as used in Ref.[9], and discuss reasons for the different results obtained. We will in addition outline how finite temperatures enters naturally the ASD theory, both from the equations of motion of of the atomistic spins[14], but also from the possibility to evaluate the inter-atomic exchange interactions at finite temperature, as demonstrated in Ref.[20]. We end this introduction with a comment that the possibility of calculating inter-atomic exchange[11] from *ab-initio* methods,is to spin-dynamics simulations, what the Hellman-Feynman force is for molecular dynamics simulations.

Before presenting a few recent applications of the Uppsala atomistic spin dynamics package, UppASD [14] on the studies of magnetic excitations in low dimensional systems we will briefly discuss magnons in other systems. The main part will be dedicated to spin-wave excitations in solids, including a few examples of dispersion curves for bulk materials and thin films.

2 Magnetic excitations in solids

When studying solids and trying to describe their properties, besides the physics of the constituent particles of the materials, like atoms or electrons, we deal also with quasiparticles. The quasiparticles can be viewed as the quanta of collective excitations. For example phonons represent the quanta of collective lattice (atoms) vibrations in a solid while magnons represent the quanta of spin-excitations. These quasiparticles behave as bosons.

Let us start by considering the simple example of a ferromagnetic spin-chain. The spins are interacting with each other via the exchange interaction, which we now consider, for simplicity, to connect only the nearest-neighbours. The only excitations that are eigenstates of the Heisenberg Hamiltonian are collective excitations, which involve a small canting of many of the spins in the system. Thus the systems enters an excited state (as can be seen in Fig. 1) where every spin will deviate from its initial equilibrium orientation, in such a way to accommodate one spin-flip over the whole spin-chain. This process will give rise to excitations that have the character of a wave, creating 'spin-waves'. In Fig. 1 we give the simple example of a ferromagnetic spin chain and its corresponding spin-wave excitation spectrum. The spin-wave excitations are characterised by a wave-vector $\vec{q}$ and energy $E(\vec{q})$, with a dispersion relation that reminds the electronic energy bands in solids. We mention here that in the limit of small wave vectors, we have a characteristic excitation energy dispersion relation relative the magnetic ordering of the systems. Thus, for a ferromagnetic material (as exemplified in Fig. 1) close to the Brillouin zone centre there is a quadratic dependency of the dispersion relation on the wavevector, while for an antiferromagnetic system, this relation is linear ($E(q) \propto q$).

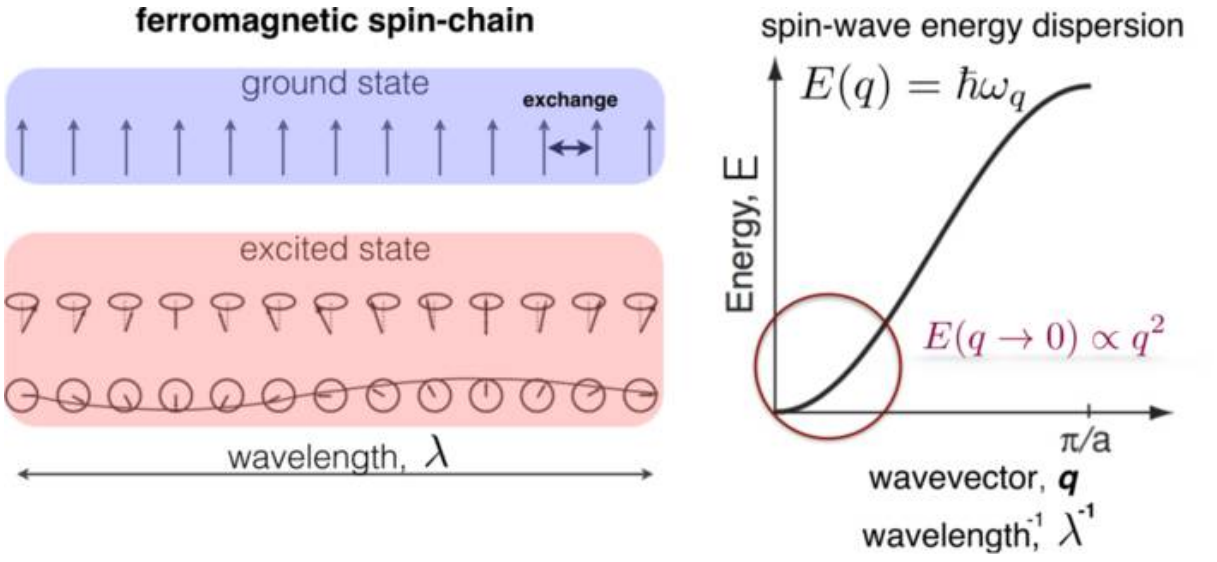

Figure 1: Simple case of a ferromagnetic spin chain in its ground state. While trying to flip one spin at one site, the energy cost is too high and the spin-flip is 'smeared' over the whole system, thus creating a so-called 'spin-wave'. This state represents an excited state of the spin chain, characterised by a wavelength λ or analogous by a wavevector q. The characteristic energy dispersion curve $E(q)$ for a ferromagnetic chain is represented on the right-hand side. (Figure adapted from Coey [21])

3 Investigation tools

We have at our disposal experimental techniques as well as theoretical methods for investigating magnetic excitations in solids. Nowadays it is possible to measure the response of magnetic systems to external stimuli, within different energy ranges and on different time scales. Moreover, theoretical models can be applied in order to simulate and predict properties and responses of different magnetic systems.

3.1 Experimental techniques

The most popular family of methods for the investigation of magnetic excitations in solids are scattering experiments. In a scattering experiment a beam of particles (neutrons, electrons, photons) is sent towards the material under investigation. The particles can collide with the system both with conservation of energy and momentum (elastic scattering) and with transfer of energy or momentum (inelastic scattering). The elastic scattering experiments give information about the underlaying structure of materials, while inelastic experiments provide insight related to the excitations created in the solid. If the incident particles gain or lose energy or momentum, this translates into the creation or annihilation of the quasiparticles characteristic to the excitations. When investigating the physics of magnetic excitations, inelastic scattering experiments represent one of the best choices. Since the scattering can be made with neutrons, electrons or light, this makes these experiments versatile, by giving us access to different length scales: e.g. probing bulk samples with neutron scattering and thin films by electron scattering. See also the diagram in Fig. 2 for a schematic representation. The inelastic neutron scattering was one of the first techniques used to determine the spin wave excitation spectra. The neutrons have a long penetration depth, thus being employed for the study of bulk materials. On the other hand, electrons have a shorter penetration depth, thus being suitable for the investigation of magnetic excitations in thin magnetic films. Thus, one can use light in Brillouin light scattering (BLS) in order to study magnetic excitations with long wavelengths (generated by dipolar interactions) or employ electrons to study short wavelength excitations, due to exchange interactions.

Moreover, we have access to a wide range of energies depending on the type of inelastic scattering experiment used (see Fig. 2). Since all experimental techniques discussed so far are based on scattering theory, it is important to analyse them in a proper theoretical framework, which involves the differential cross section and the dynamical structure function. The latter will be discussed in this manuscript in some detail.

3.2 Theoretical methods

Besides the different experimental techniques, for the study of magnetic excitations in solids, we have at our disposal different theoretical approaches as well: mathematical models and computer simulations. An important tool is represented by theoretical simulations, due to their strong predictive power and capability to be materials specific. By employing computer simulations, we can make predictions regarding the properties of different materials or even design materials with desired features. Establishing the link between experiments and theoretical methods allows us to

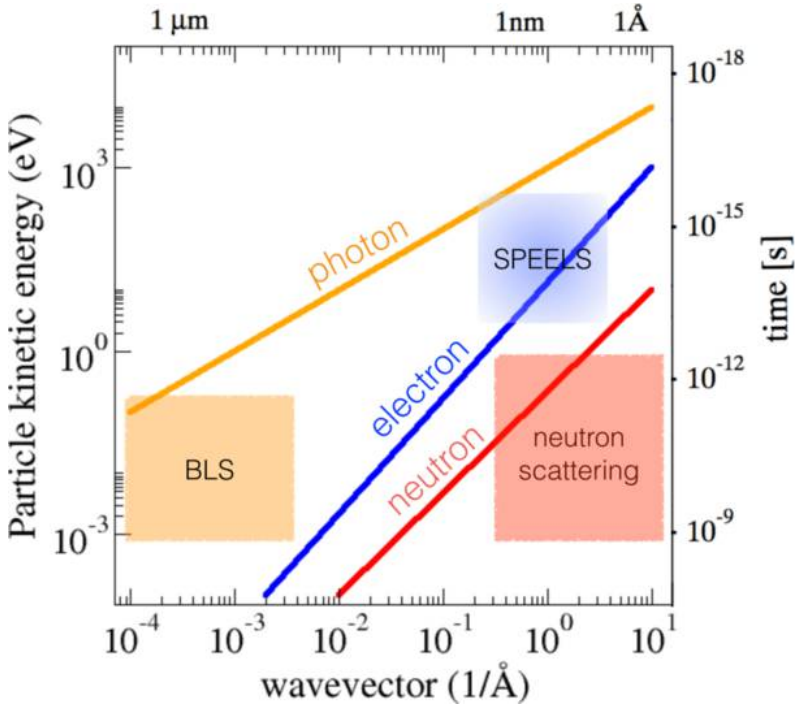

Figure 2: Energy and momentum transfer range achieved in inelastic scattering experiments when using: photons, electrons or neutrons. Diagram reproduced from Refs. [22] and [23].

understand better the experimental results and get a deeper insight into the physical phenomena. In the same time, this leads to a constant improvement of the theoretical tools as well.

One way of estimating the spin-wave excitation spectra is by employing the frozen magnon approach [24, 25, 5]. This method consists in performing first principles spin-spiral calculations. For each calculation, a different spin-spiral is considered to be fixed in the system, thus the name 'frozen magnon'. For each case the total energy of the system is calculated and the excitation energy is determined by the total energy differences between different cases (each case represented by a different spin-spiral). Another method for the simulation of magnetic excitations in solids, consists in calculating the dynamical susceptibility of magnetic systems. Different groups use slightly different approaches for determining the dynamical susceptibility and to simulate the magnon spectra. Different versions of this method is described in the work of Cooke et al. [26], Savrasov et al. [27], Costa and Mills [28] and references therein. We mention here the approach employed by Costa et al. [28, 29] that leads to the determination of the magnon dispersion spectra. In their approach, the description of the ground-state properties of the system is made by a tight-binding method with parameters extracted from fitting the *ab initio* bulk electronic structure. Additionally, Costa et al. employ a one-parameter scheme where the Coulomb interaction (U) value can also be modified. They describe the spin waves excitations spectra by means of the random phase approximation (RPA), calculating the transverse frequency dependent susceptibility. The main difference between the adiabatic magnon approximation and the RPA method regards the treatment of the particle-hole excitations. These excitations, known also as Stoner excitations, [30] are neglected in the adiabatic case. They are not relevant at low energies but can become significant at higher energies or large wave-vectors. Therefore one would

expect theories based on the adiabatic approach to break down at the Brillouin zone boundary. Similar to the method described above, another approach for the determination of magnetic excitations is by calculating the dynamical susceptibility within linear response time-dependent density functional theory [31, 32].

Focusing now on the ASD method, our theoretical investigation of magnetic excitations is performed within a *multi-code* and *multi-scale* approach. The systems of interest are investigated by means of *ab initio* density functional theory (DFT) methods and atomistic spin dynamics (ASD) [14], e.g. as provided in the UppASD (Uppsala Atomistic Spin Dynamics) package. The first step is represented by the determination of the ground-state properties of the system by means of *ab initio* calculations. We shall describe this first step in detail in Section 3.3. In the second step, the quantities calculated by *ab initio* methods are used as input for atomistic spin dynamics simulations, see Section 3.4, by using the *ab initio* magnetic moments, exchange parameters, Dzyaloshinskii-Moriya interactions and anisotropies mapped onto a spin-Hamiltonian. We then employ the atomistic Landau-Lifshitz-Gilbert equation and evaluate the dynamical structure factor (the quantity which is accessible in scattering experiments). From the dynamical structure factor we then identify the spin-wave excitation spectra as they would appear in a scattering experiment.

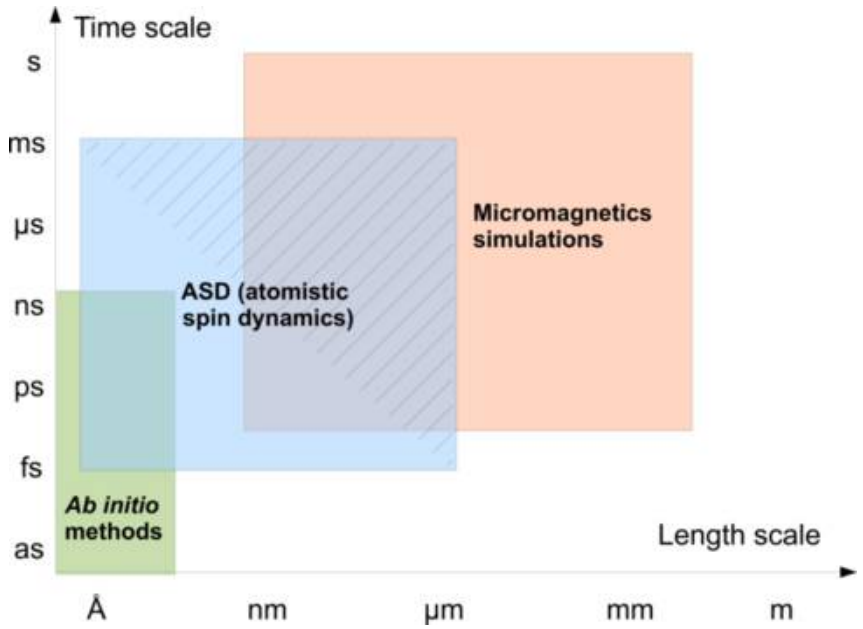

Figure 3: Bridging the gap: the ASD link between *ab initio* methods and micromagnetics simulations.

This means that the static and dynamic magnetic properties are being studied with different techniques and computational methods, at the subatomic level (first principles) as well as on a larger scale up to almost micrometer level (in ASD). Investigations of the dynamics for large systems (micrometers) or for longer observation times (nanoseconds) is possible with the massively parallelised version of the UppASD package.

Maybe the most accurate way of treating magnetisation dynamics is from first principles by means of the time-dependent magnetisation density functional theory (TD-SDFT) or time-

dependent current density functional theory (TD-CDFT). However, both TD-SDFT and TD-CDFT work best for finite systems and are not yet efficient for extended systems. Another well established method which addresses and describes the magnetisation dynamics are micromagnetic simulations (valid for time-scales longer than 1 ps (picosecond) and length-scales larger than nanometers). In micromagnetism, the system of interest is divided in domains which are approximated by macro-spins and their dynamics described by the phenomenological Landau-Lifshitz-Gilbert equation. As is sketched in Fig. 3, the ASD method fills the gap between TD-DFT and micromagnetics, acting on sub-picosecond time-scales and on a sub-nanometer length scale, by treating atomic moments instead of spin density.

3.3 First Principles Calculations

Whenever one is interested in investigating magnetic excitations in solids, in the first step of the study a thorough description of the ground state properties of the system is given by employing various first-principles methods. The *ab initio* codes frequently used here are the Vienna Ab-initio Software Package (VASP) [33, 34] and codes based on the Korringa-Kohn-Rostoker (KKR) [35, 36] method within multiple scattering theory (MST). First we set-up the system: bulk, surface or multi-layers. For magnetic multi-layers we use a slab representing the substrate, having on one side the magnetic over-layer and a large region of vacuum, simulating the surface. The interlayer distances are relaxed according to the forces using the projector augmented wave method (PAW) as implemented in the VASP program [33, 34]. After obtaining the optimised (relaxed) geometry, the Heisenberg exchange interactions are calculated e.g. by KKR or real-space LMTO methods. We frequently employ either RS-LMTO-ASA or the SPR-KKR package [36, 37]. In the latter, Green's functions formalism is used and the Kohn-Sham-Dirac equation is solved, which means that we have a fully relativistic formulation of the problem at hand: accounting for relativistic effects, such as the spin-orbit coupling (SOC). In this way we can access a large set of *ab initio* calculated quantities (spin and orbital moments, magnetic anisotropies, exchange interactions, Dzyaloshinkii-Moryia interactions), thus fully characterising the system of interest in its ground-state. In most of the examples presented in this review, we used the local spin density approximation (LSDA) for the exchange-correlation potential and a basis set consisting of s, p, d and f orbitals. For the self-consistent calculations we typically employ between 4-500 k-points in the two dimensional Brillouin zone, while a much more dense k-point grid of 2000 k-points is used in the calculation of Heisenberg exchange parameters and Dzyaloshinskii-Moriya interactions, sufficient to obtain a convergence on a microRydberg level for these parameters. All these quantities (magnetic moments and exchange) are later used within a generalised Hamiltonian for atomic spin dynamics simulations.

The exchange parameters J_{ij} and Dzyaloshinskii-Moriya (DM) vectors $\mathbf{D}_{ij}$ are obtained from the relativistic generalisation [38, 39] of the real-space method of infinitesimal rotations of Liechtenstein, Katsnelson and Gubanov (LKG) [11, 40] with the ferromagnetic configuration chosen as the reference state for mapping. We calculate the full exchange tensor $\bar{J}_{ij}$ is calculated. This can be decomposed into its isotropic part J_{ij} and its anti-symmetric part, which corresponds to the DM-vectors.

Having calculated the exchange parameters J_{ij}, they can be Fourier transformed to obtain the

so-called adiabatic magnon spectrum. In the simple case of a single layer (corresponding to one atom per cell), the energy of a spin wave with respect to a ferromagnetic ground state is given by

$$E(\mathbf{q}) = \sum_{j \neq 0} J_{0j} \left[\exp\left(i\mathbf{q} \cdot \mathbf{R}_{0j} \right) - 1 \right], \tag{1}$$

where $\mathbf{R}_{ij}$ is the relative position vector connecting sites i and j. From this it is straightforward to calculate the spin wave dispersion $\omega(\mathbf{q})$. [5] For systems with more than one atom per cell, as is the case for thin films consisting of more than one monolayer, the spin wave energies are given by the eigenvalues of the general $N \times N$ matrix here expressed in block form

$$\begin{bmatrix} \sum_j^N J_0^{ij} - J^{ii}(\mathbf{q}) & -J^{ij}(\mathbf{q}) \\ -J^{ij}(\mathbf{q})^* & \sum_i^N J_0^{ji} - J^{jj}(\mathbf{q}) \end{bmatrix}, \tag{2}$$

where N is the number of atoms per cell (*i.e.* in this case the number of magnetic layers). The whole procedure relies on an adiabatic approximation in which the slow motion of the spins is decoupled from the fast motion of the itinerant electrons, a situation that is justified at low energy scales and for systems with reasonably large exchange splitting.

Adiabatic magnon spectra

As mentioned above, by applying a Fourier transformation on the exchange parameters obtained from first principles calculations, we are able to generate the adiabatic magnon dispersion spectra. Below we shall present a few examples of such spectra both for bulk materials as well as for thin magnetic layers.

Bulk systems

In Fig. 4, we reproduce the results obtained by Halilov et al. [25] for bulk Co. In Fig. 4(a), Co is present in the face-centred cubic crystal structure which is a Bravais lattice, namely having one-atom per unit cell. As discussed in the previous section, this gives rise to one branch in the spin-wave excitation spectra. When dealing with non-primitive lattices, such as hexagonal-closed-packed structures, which have two atoms per unit cell as shown in Fig. 4(b), there are two branches that appear in the magnon spectra. From analogy to phonons dispersion, the lowest-laying branch is called 'acoustic' branch while the branches appearing at higher energies are denoted as 'optical' branches.

Thin films

Fig. 5(a) displays the calculated adiabatic magnon spectrum obtained for 8 ML Co/Cu(001), using Eq. (2) with J_{ij} values obtained using the LKG method. [11, 40] The most notable feature is the presence of several branches, one for each Co layer present. This is in contrast to experimental observations, where only the lowest ("acoustic") branch [41] (filled circles in Fig 4) as well as

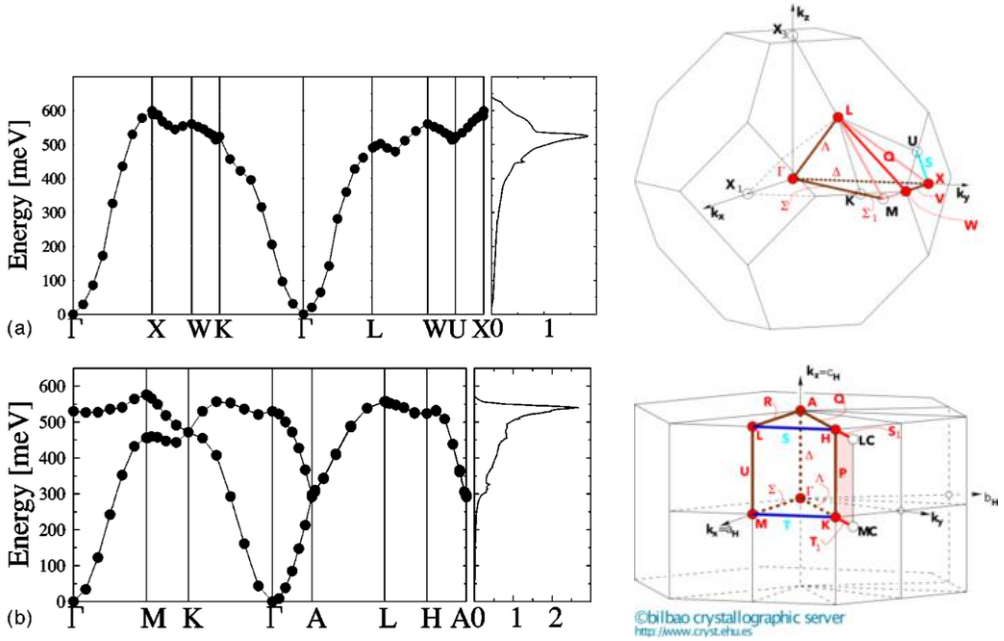

Figure 4: Adiabatic magnon spectra for (a) fcc bulk Co and (b) hcp bulk Co as calculated by Halilov et al. [25].[Fig.4 reprinted from Ref. [25]]. On the right-hand side panel, the corresponding Brillouin zones are represented, together with the high-symmetry points and lines.

the second lowest branch [29] are observed. Vollmer *et al.* [41] conclude that this indicates the shortcomings of a direct interpretation of their data in terms of a naïve Heisenberg model.

Fig. 5(b) displays the adiabatic magnon spectrum obtained for 3 ML Fe/Cu(001). Unfortunately, there are no experimental data to compare with. The values for the spin wave stiffness, D, can be estimated from the calculated adiabatic magnon spectra by measuring the curvature of the dispersions as $\mathbf{q} \to 0$. For this system we find D being approximately 210 meV Å^2. For the 1 ML Co on Cu(001) case we obtain a value of the order of 420 meV Å^2 - a 15 % overestimate of the experimentally determined value of 360 meV Å^2, but considerably softer than the theoretical value determined by Pajda *et al.* [42] of 532 ± 9 meV Å^2 obtained by a real-space adiabatic approach. For 1 ML Fe on Cu(001) we obtain a lower value, of 260 meV Å^2 compared to the value of 331 meV Å^2 by Pajda *et al.* [42].

In Fig. 6 we present the simulated adiabatic magnon spectra for a system with 6 layers of Fe on Ir(001), together with very recent experimental data [9] obtain by SPEELS. The experimental points have been taken from Fig.2 in Ref. [9].

3.4 Atomistic Spin Dynamics

The set of site-resolved *ab initio* parameters (including spin and orbital moments, magnetic anisotropies, exchange interactions and Dzyaloshinkii-Moryia interactions) obtained in this way is used as a starting point for the spin dynamics simulations. In order to study the magnetisation dynamics, we employ atomistic spin dynamics simulations, in the step that follows the electronic structure part of each investigation. In practice, the first step of our approach is to map the itinerant electron system onto an effective Heisenberg Hamiltonian with classical spins:

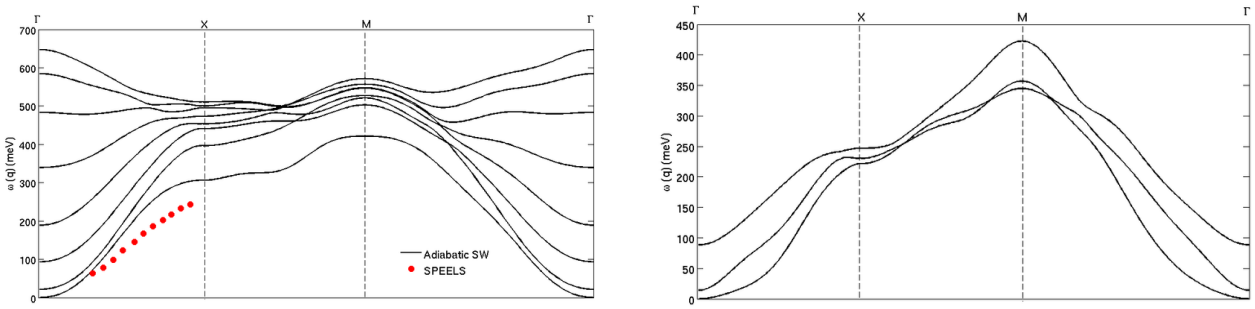

Figure 5: : (Color online) Adiabatic magnon spectra (full lines) obtained from SPR-KKR calculations for (a) 8 ML Co/Cu(001) together with experimental SPEELS data [41] (circles) and (b) 3 ML Fe/Cu(001).

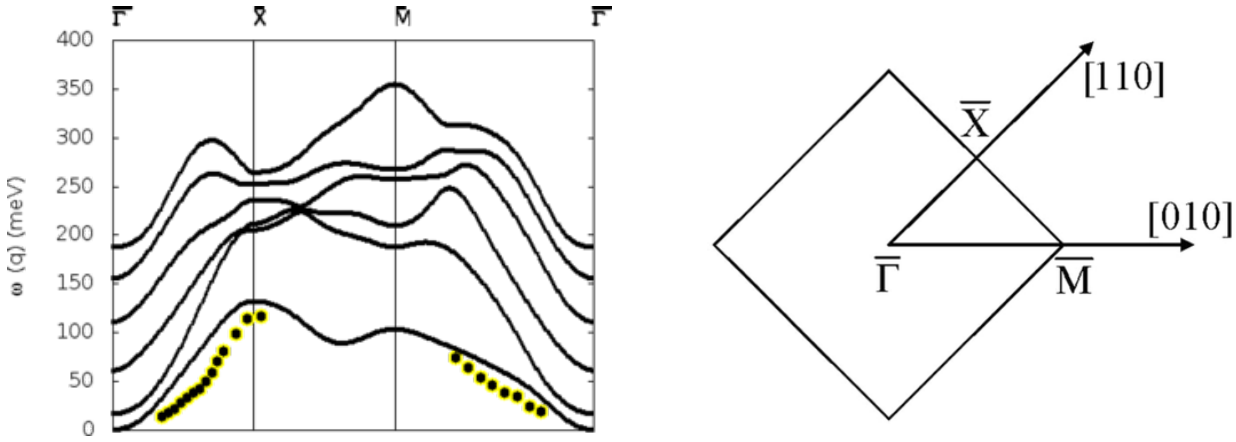

Figure 6: (colour online) Adiabatic magnon spectra (full lines) obtained from SPR-KKR calculations for 6 ML Fe/Ir(001). The black dots represent recent experimental data obtained by SPEELS [9]. On the right hand side, the corresponding surface Brillouin zone is represented, where we specify the high-symmetry points.

$$\mathcal{H} = \underbrace{-\frac{1}{2}\sum_{i\neq j} J_{ij}\vec{m}_i\cdot\vec{m}_j}_{exchange} + \underbrace{\sum_i K_i(\vec{m}_i\cdot\vec{e}_K)^2}_{anisotropy} \underbrace{-\frac{1}{2}\sum_{i\neq j} Q_{ij}^{\mu\nu} m_i^\mu m_j^\nu}_{dipolar} + \underbrace{\sum_{i,j}\tilde{D}_{ij}(\vec{m}_i\times\vec{m}_j)}_{Dzyaloshinskii-Moryia} \underbrace{-\vec{B}_{ext}\cdot\sum_i \vec{m}_i}_{external},$$

which includes exchange interactions J_{ij}, anisotropies K_i, dipolar interactions $Q_{ij}^{\mu\nu}$, Dzyaloshiskii-Moriya (DM) vectors [43, 44] $\tilde{D}_{ij}$ and the Zeeman term $B_{ext}\cdot m$, where m_i represents the magnetic moment vector and B_{ext} is the applied magnetic field. The exchange integrals, spin moments, anisotropies etc. are obtained, as mentioned before, from *first principles* calculations. UppASD may be used a material specific method which can treat arbitrary types of magnetic ordering (ferromagnetic, antiferromagnetic, helimagnets etc) or start from random magnetic configurations.

Within the adiabatic approximation, we separate the fast variables (the electrons) from the slow variables (the atomic moments), and the equation of motion for the atomic spins is given in

terms of the atomistic Landau-Lifshitz-Gilbert (LLG) equation, as derived in Ref. [12]:

$$\frac{\partial \vec{m}_i}{\partial t} = \underbrace{-\frac{\gamma}{1+\alpha^2}\,\vec{m}_i \times \vec{B}_i^{eff}}_{precession} \underbrace{-\frac{\gamma}{1+\alpha^2}\,\frac{\alpha}{m}[\vec{m}_i \times [\vec{m}_i \times \vec{B}_i^{eff}]]}_{damping}. \tag{3}$$

The temporal evolution of the atomic spins at finite temperature is governed by Langevin dynamics, through coupled stochastic differential equations, the Landau-Lifshitz-Gilbert (LLG) equations, written here in the Landau-Lifshitz form (Eq. 3).

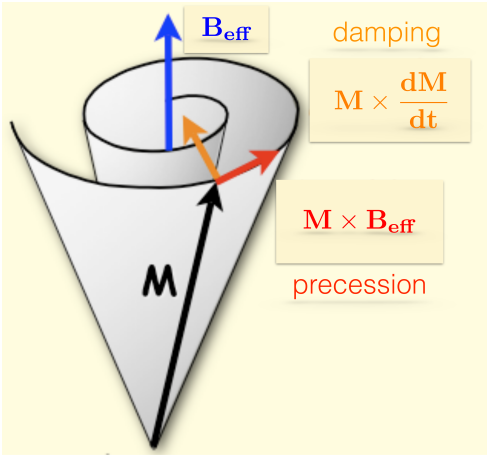

Figure 7: Schematic representation of the torques acting on each individual spin, according to Eq. 3.

In LLG we have a damping parameter α present. γ represents the gyromagnetic ratio. The determination of the proper damping is a problem in itself. There have been several efforts in calculating the damping parameter from first principles theory [45, 46, 47, 48, 49], with overall encouraging results when compared to experimental data. However, more experience is needed before one can conclude how realistic one-electron theory can capture the damping parameter, which in principle should be a tensorial quantity, material specific and depending on both temperature and frequency.

In the second step of the simulation, we evolve the effective field $\vec{B}^{eff}$ for each individual atomic moment according to the LLG equation of motion:

$$\vec{B}_i^{eff} = -\frac{\partial \mathcal{H}}{\partial \vec{m}_i}\,, \text{where} \quad \vec{B}_i^{eff} = \vec{B}_i + \vec{B}_i^{fl}(t) \tag{4}$$

The finite temperature effects are included in the fluctuating (stochastic) magnetic fields $\vec{B}_i^{fl}(t)$, via Langevin dynamics. The Langevin approach gives a more concrete description than the Fokker-Planck equation, but it is mathematically equivalent to it [50].

Temperature fluctuations are included via a stochastic Gaussian shaped magnetic field $B_i^{fl}(t)$ with properties $\langle \vec{B}_i^{fl}(t) \rangle = 0$ and

$$\langle B_i^{fl,k}(t) B_j^{fl,l}(t') \rangle = 2D\delta_{ij}\delta_{kl}\delta(t-t'), \qquad D = \frac{\alpha}{(1+\alpha^2)}\frac{k_B T}{\mu_B m}, \tag{5}$$

where i and j denote lattice sites, k and l the carteisian components and α is the Gilbert damping parameter which eventually brings the system to thermal equilibrium. It should be noted that the simulations carried out in this work are for atomistic spins. Hence the gyromagnetic factor in this simulations is simply the ratio between the magnetic moment and the angular momentum of an atom. An anisotropy in the gyromagnetic factor, with respect to the orientation of the atomic spin, would appear in the first principles part of our calculation, where the spin and orbital magnetic moments are calculated. It is known that this effect is rather small for transition metals (e.g. as reported by Hjortstam *et al.* [51] and Stöhr [52]). The dependence on any possible anisotropy of the damping parameter is less known. However, for most of our calculations the thermal fluctuations do not force the moments to deviate too much from the easy magnetisation axis, and hence a possible tensorial form of the damping parameter would not influence our results by a significant amount.

The coupled equations of motion (3) can be viewed as describing the precession of each spin about an effective interaction field, with complexity arising from the fact that, since all spins are moving, the effective field is not static. In our calculations we evolve the stochastic LLG equations using a semi-implicit method introduced by Mentink *et al.* [53]

The principal advantage of combining first-principles calculations with the ASD approach is that it allows us to address the dynamical properties of spin systems at finite temperatures. [14, 54, 55] We focus in particular on two important quantities, the space- and time-displaced correlation function:

$$C^k(\mathbf{r}-\mathbf{r}',t) = \langle m^k_{\mathbf{r}}(t) m^k_{\mathbf{r}'}(0)\rangle - \langle m^k_{\mathbf{r}}(t)\rangle\langle m^k_{\mathbf{r}'}(0)\rangle, \tag{6}$$

where the angular brackets signify an ensemble average and k the cartesian component, and its Fourier Transform, the dynamical structure factor:

$$S^k(\mathbf{q},\omega) = \frac{1}{\sqrt{2\pi}N}\sum_{\mathbf{r},\mathbf{r}'} e^{i\mathbf{q}\cdot(\mathbf{r}-\mathbf{r}')}\int_{-\infty}^{\infty} e^{i\omega t} C^k(\mathbf{r}-\mathbf{r}',t)dt, \tag{7}$$

where $\mathbf{q}$ and ω are the momentum and energy transfer, respectively. The dynamical structure factor, $S(\mathbf{q},\omega)$ is the quantity probed in neutron scattering experiments of e.g. bulk systems [56], is analogously applied here to interpret SPEELS measurements. By plotting the peak positions of the structure factor along particular directions in reciprocal space, the spin wave dispersions as they would appear in a scattering experiment, may be obtained. [16, 14, 54, 55]

All codes/methods used, the KKR, the real-space LMTO electronic structure methods, as well as the UppASD spin-dynamics method, are versatile and their performances have been tested on a wide range of systems and properties (see [57, 35] and [14, 58, 16] and references therein). We have recently done a massive parallell implementation using MPI of the UppASD program that allow the treatment of much larger structures (nm to μ m) and longer observation times. We have so far tested the program with good scalability for systems with $\geq 1.5\cdot 10^9$ atoms running on 13 824 processors on a Cray XE6 supercomputer. In addition, we have also ported the program to graphics processors units (GPU) using the CUDA framework with promising scalability.

4 Spin-waves excitation spectra from atomistic spin-dynamics simulations

4.1 Bulk ferromagnets

As a first demonstration of our methodology we start with the well studied materials Fe and Co. There are plenty of measured and calculated magnon dispersions for these materials published in the literature, in this context it is worth mentioning the frozen magnon calculations by Halilov *et. al* [25] based on direct spin spirals configurations in reciprocal space and alternatively, if exchange interactions calculated in real space are Fourier transformed, it yields the adiabatic magnon dispersions, a method that has been employed by Pajda *et. al.* [42] and others. Another method that has been employed recently and differs a bit from the other mentioned are calculations of the Kohn Sham susceptibility through linear response and from that estimation of the magnon dispersion. The strength of this method is that it includes longitudinal fluctuations on the same footing as transversal fluctuations but to the expense of time consuming calculations restricting the method so far to simple systems.

Our methodology, as outlined in Section 3.4, is much in line with the second method mentioned above, namely we first calculate exchange interactions (and related parameters) but instead of a direct Fourier transform we perform spin dynamics calculations at finite temperature and from the induced fluctuations we obtain the excitation spectra through the dynamical structure factor.

In Figure. 8 the calculated magnon dispersion spectra of bcc Fe at T=10 K is displayed with a damping parameter $\alpha = 0.003$, all the other interactions were calculated from first principles theory. As expected from the low temperature and damping, the overall spectra is in good agreement with previous adiabatic calculations and also experiment and in particular the theory captures the onset of a Kohn anomaly in the $\Gamma - H$ direction arising from long range exchange interactions (in the simulations all interactions up to $R_{max} = 7 \times a_{lat}$ were included). As known for ferromagnets close to the Γ-point, the magnon dispersion follows the relation $\omega(\mathbf{q}) \approx Dq^2$, where D is the exchange spin wave stiffness constant. Extracting value of D is however a very delicate matter due to the oscillatory behaviour of the exchange interactions in bcc Fe. Following the procedure as outlined in Ref.[59] and complementary calculations from direct fitting of the magnon dispersion gives value of D $\approx$ 270 meVÅ^2, which is in fair agreement with the experimental value of 314 meVÅ^2 [60].

In Figure 9 we show the magnon dispersion calculated for hcp Co at T=10 K and $\alpha = 0.003$. Since there are two atoms in the hcp unit cell, two magnon branches are expected.In order to sample both branches, the momentum transfer need to be varied as it is often done in neutron scattering and discussed in Section.4.1. If the sampled wave vectors $\mathbf{q}$ are confined in the first Brillouin zone, Fig.9(a), the intensity of the dynamical structure factor is dominated by the acoustic branch. By varying the momentum transfer, for instance shifting the sampled wave vectors outside the first Brillouin zone, Fig.9(b), the intensity of the dynamical structure factor is reversed so that the optical branch dominates. This is analysed in more detail below.

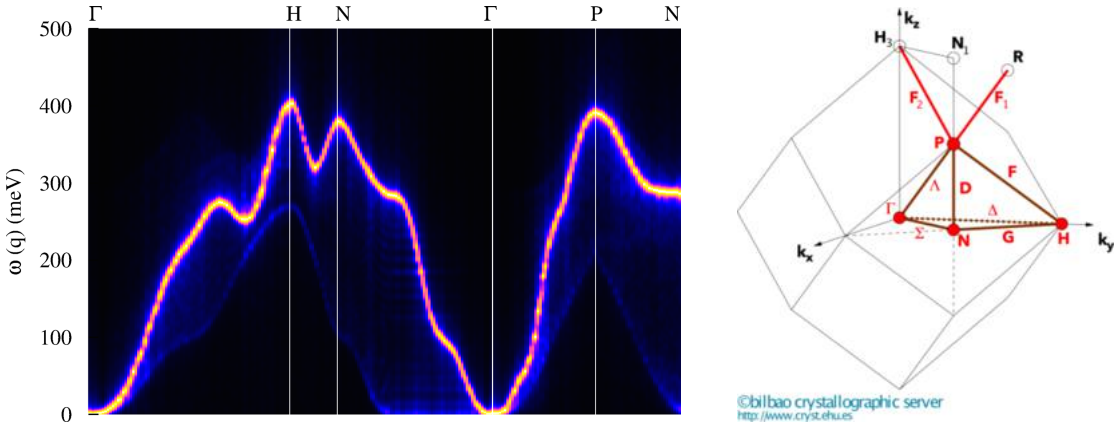

Figure 8: (Color online) Calculated magnon dispersion spectra for bcc Fe at T=10 K and the corresponding Brillouin zone.

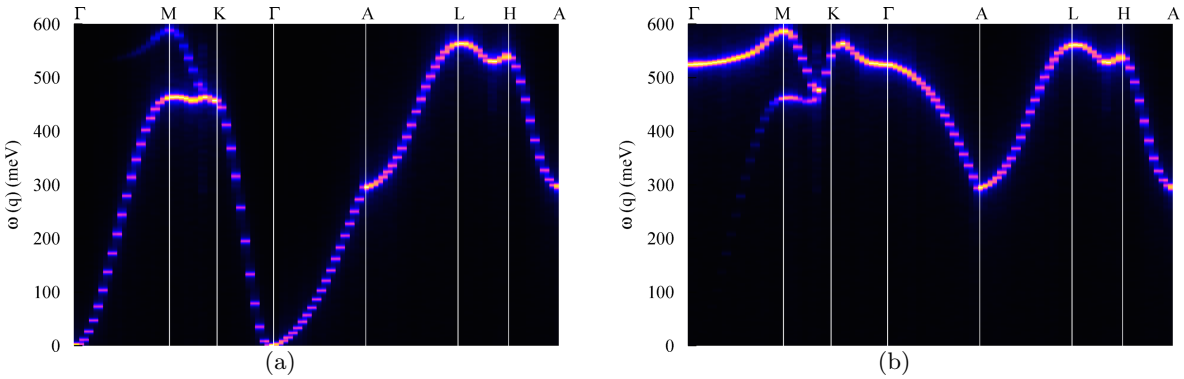

Figure 9: (Color online) Magnon dispersion of hcp Co at T=10 K from atomistic spin dynamics. In (a) q-vectors in the first Brillouin zone and in (b) q-vectors shifted by $\mathbf{b_3}$ were sampled where $\mathbf{b_3}$ is a reciprocal lattice vector in c-direction.

Analysis of the dynamical structure factor

In the analysis of magnon dispersions as obtained from neutron scattering, the susceptibility was shown to be written in the following form [61]

$$\bar{\bar{\chi}}(\boldsymbol{q}+\boldsymbol{\tau},\omega) = \frac{1}{2}(1+\cos\phi)\bar{\bar{\chi}}_{Ac}(\boldsymbol{q},\omega) + \frac{1}{2}(1-\cos\phi)\bar{\bar{\chi}}_{Op}(\boldsymbol{q},\omega), \tag{8}$$

where $\bar{\bar{\chi}}_{Ac}$ and $\bar{\bar{\chi}}_{Op}$ are the susceptibilites originating from accoustic and optical branch, respectively, $\boldsymbol{q}$ is a reciprocal vector within the primitive Brillouin zone (BZ), $\boldsymbol{\tau} = [hkl] = h\boldsymbol{b}_1 + k\boldsymbol{b}_2 + l\boldsymbol{b}_3$, $\phi = \boldsymbol{\tau}\cdot\boldsymbol{\rho}$, where $\boldsymbol{\rho}$ is a vector connecting two sublattices. In this manner, by changing the momentum transfer by varying $\boldsymbol{\tau}$, the intensity of the accoustic and optical branches is changing. If we take the hcp Co as an example, $\boldsymbol{\rho} = [0\ 0\ 0.5]c$ and it follows that $\boldsymbol{\phi} = l\pi$. Inside the primitive BZ, the phase $\phi = 0$ and in the limit $\boldsymbol{q} \to \mathbf{0}$, in Eq. (8) the acoustic term will dominate and will be detected in experiment. If we go outside the first BZ, it is possible to have a situation where the optical term dominates, on the expense of the acoustic response, for instance by choosing $\boldsymbol{\tau} = [001]$, as illustrated in Fig. 9(b). If there are more than

two atoms in the unit cell, the analysis becomes more complicated but the principle is the same.

4.2 Bulk antiferromagnets

As a prototype for a bulk antiferromagnet we choose the transition metal oxide NiO. The transition metal oxides (TMO) are well studied in the context of density functional theory since in order to reproduce the antiferromagnetic order and the formation of a gap in the electronic band structure, correlation effects must be included beyond the local density approximation (LDA). The most straight forward method that works reasonably is the LDA+U approximation, which goes back to Lopez-Aquilar and C. Quintana [62] in 1984 and Anisimov [63] in 1991 that adds a Hubbard-like term on top of the LDA. For "typical" values of the Hubbard U (4-8 eV) , the electronic band structure agrees rather well with experimental observations and the ground state is antiferromagnetic. We performed LDA+U calculations using the SPR-KKR program in scalar relativistic mode and full potential. U was varied between 4-8 eV and exchange constants were calculated up to arbitrary distance, however the exchange interactions are rather short ranged due to the presence of a gap that acts as an additional screening. The exchange interactions are rather dependent on choice of U value and here we show only results for U=7 eV that yields a calculated Neel temperature using Monte Carlo simulations of $\approx$ 390 K which is underestimated compare to experimental value of 523 K. However, it is worth noting that decreasing U to 4 eV yields to calculated Neel temperature of 520 K in good agreement with experimental value.

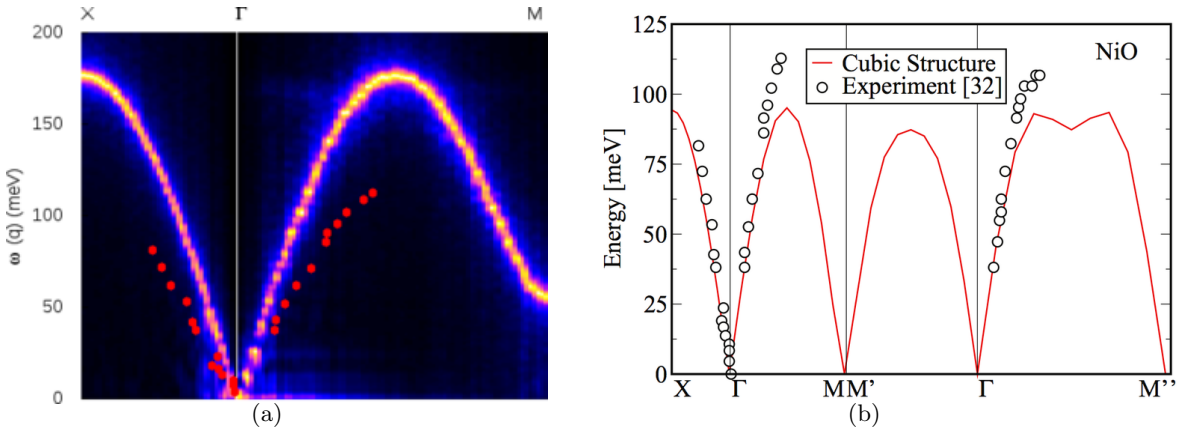

Figure 10: (Color online) (a) Simulated spin wave spectra for antiferromagnetic NiO at T=10 K using LDA+U approximation with U=7 eV. (b) Adiabatic magnon spectra for NiO as published by Jacobsson et al. [64], calculated using the FLEUR code, within LDA+U for U=8 eV. (reprinted Fig.9 from [64]) The experimental data correspond to results published in Ref. [65].

In general, the values of the exchange parameters for transition metal oxides depend quite strongly on the exchange-functional used in the calculation, and consequently the spin-waves excitation spectra reflects this dependency. We show in Fig. 10(a) the example of magnon spectra for NiO, simulation from atomistic spin dynamics at T=10K and damping $\alpha = 0.01$ using with exchange parameters calculated with SPR-KKR within LDA+U, with U=7 eV. As we can notice, with the chosen value of U, the magnon dispersion is slightly overestimated and reaches higher energies than the experimentally measured excitation[65]. Recent studies [66, 64] have shown that there is a strong dependence of the exchange parameters on the value of U

used in the calculations. As an example in Fig 10(b), we chose to reprint Fig.9 from Ref. [64] which represents the calculated adiabatic magnon spectra for NiO. The calculation has been performed the FLEUR code and within LDA+U for a value of U=8 eV. For the chosen U-value, the exchange parameters are slightly underestimated and the calculated magnon mode lays at lower energies than the experimental data. For a detailed investigation of the exchange parameter dependence on the value of U, we refer the reader to the above mentioned study [64].

4.3 Ferromagnetic thin-films

Even though the bulk spin-wave excitations spectra have been accessible to experimental investigations for many decades, the study of magnon dispersion curves for thin films is a recent achievement for both experiment and theory. Moreover, the reduced dimensionality of the systems (2D of thin films vs. 3D of bulk) leads to unexpected and sometimes exotic phenomena: non-collinear or frustrated magnetic order, chiral states and broken time-reversal symmetry etc.

4.3.1 Fe on W(110)

In an excellent demonstration of the capabilities of the SPEELS method, Prokop and co-workers [7] were able to apply the method to a single magnetic layer. The considered system was a monolayer of Fe on W(110), a prototypical low-dimensional ferromagnetic system that has earlier been studied by a number of different experimental methods[67, 68]. In addition to showing the possibility to probe magnons in magnetic monolayers, the main result found by Prokop et al. was that the measured magnon energies were significantly softened compared to bulk magnons. This observed softening was also found to be in strong contrast with previous theoretical RPA based calculations [69] of the system, despite the fact that similar calculations [29] have earlier agreed quite well with SPEELS results. In order to address the observed discrepancy between theory and experiment, the system was studied by a combination of first principles calculations and ASD simulations [16].

The first-principles calculations based on KKR and LMTO theory showed that while the magnetic order of the ML of Fe on W(110) was indeed ferromagnetic, it was only quite weakly so. Calculated exchange interactions showed that these interactions were long-ranged but also slightly frustrated where especially the next-nearest neighbor coupling favored an anti-ferromagnetic arrangement of the magnetic moments. Depending on the cut-off of the exchange interactions and on the numerical details of the first principles calculations, the weak and slightly frustrated exchange interactions would actually, in some situations, tend to favour a non-collinear spin-spiral ground-state ordering of the Fe moments, which was also noticed in an earlier theoretical investigation[70]. The weak ferromagnetic ordering driven by the exchange interactions, is also strengthened by the strong magnetocrystalline anisotropy energy occurring in the system. Enhanced by the heavy substrate, the MAE for the system is 4.2 meV/atom and favors an easy axis in the film plane.

Already from the calculated exchange parameters, a notable softening of the exchange compared with bulk Fe was noticed and could be explained in terms of the geometry and hybridisation effects with the W(110) substrate. However, to further examine the effect of thermal fluctuations on the magnon spectra, ASD simulations were performed using the calculated exchange param-

eters. As it is well known, one of the limitations of the Heisenberg model is that the exchange interactions J_{ij}, which are approximated to be constant in the model, are actually depending on the reference configuration for which the interaction parameters are calculated from. While this is a draw-back of methods based on the Heisenberg Hamiltonian, it actually also gives an opportunity to model the effect of finite temperatures on the exchange interactions. Typically that is used by comparing exchange strengths calculated from ferromagnetic reference states, which would correspond to zero temperature, with interactions calculated from a disordered non-collinear reference state that would then emulate interactions at high temperatures. Typically, the disordered high-temperature state is modelled using the coherent potential approximation (CPA) for collinear but random magnetic disorder which results in the disordered local moments approximation (DLM). In Ref. [16] both ferromagnetic and fully disordered reference states were considered but also a partially disordered state was modelled by means of uncompensated, or partial, DLM configurations (pDLM). The idea with pDLM is that by not considering a 50-50 up/down spin configuration, one should shift the relation so that a finite but reduced net magnetisation is present in the calculation of the exchange interactions. By comparing with the average magnetisation for a given temperature T, a suitable pDLM ratio which correspond to the same magnetisation can be chosen and assumed to be a good description of the temperature present in the system. The pDLM concept has earlier in other situations and a recent systematic investigation of the approach can be found in Ref.[71].

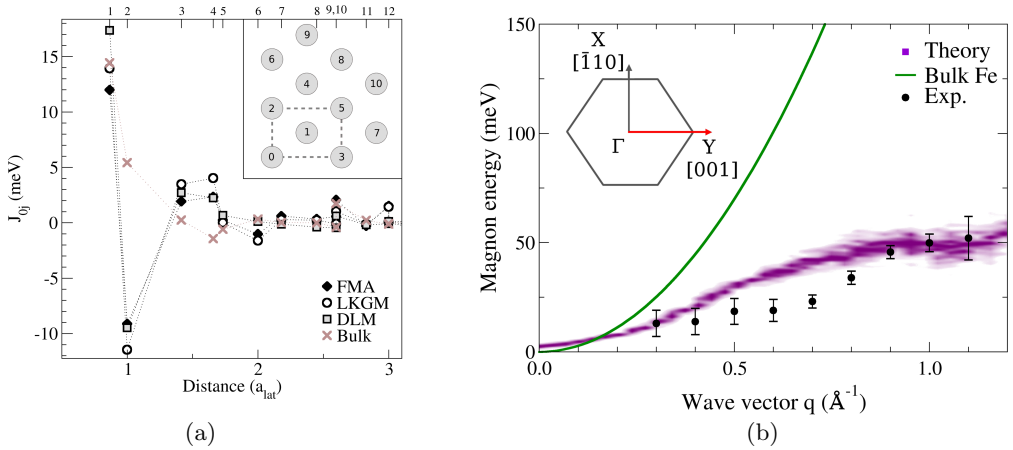

Figure 11: (a) Calculated exchange interaction parameters J_{ij} for a ML Fe on W(110) as a function of distance (in lattice constant a_{lat}). The J_{ij}s labelled FMA were obtained using the "frozen magnon" approximation while the other curves was calculated using the LKGM method for a ferromagnetic solution (LKGM), and disordered local moment state (DLM). Also shown are the calculated exchange interaction parameters for bulk bcc Fe. The inset shows the geometry of the ML and position of neighbour j relative to site 0. (b) Comparison between magnon dispersion curves along the [001] direction for a ML Fe on W(110). The dots are experimentally obtained data [7], whereas the thick purple line represents our numerically obtained data. For comparison, the experimental spin wave spectrum of bulk bcc Fe (corresponding to a spin wave stiffness constant of 280 meV Å^2) [72] is also displayed.

As the magnon spectra for the Fe/W(110) system was measured at 120K, a pDLM configuration

corresponding to a magnetisation of 85% of the saturation magnetisation was used to calculate exchange parameters for the ASD simulations and it was found that the pDLM interactions gave an additionally softened magnon spectra compared with the exchange interactions calculated from the low-temperature ferromagnetic reference state. The thermal fluctuations in the simulations, which are governed by Langevin dynamics also gave rise to further softening of the magnon spectra. In conclusion, the simulated magnon spectra was in good agreement with the measured data, and the combined first-principles calculations and atomistic simulations could provide an answer to the previously unexplained softening of the magnons as a combination of the effect of the electronic structure of the ML system with finite temperature effects [16].

In the section above, we discussed data of the calculated [16] spin wave spectra of a single Fe layer on top of W(110) and compared it with the experimentally determined spectra [7] and found a good agreement.

We now turn our attention to the magnons of a Fe bilayer on W(110). Experimentally, the magnon dispersion has been measured by SPEELS [73] where in addition the magnon lifetimes were determined [74]. In Fig. 12 we show our calculated magnon dispersion along symmetry lines in the first Brilloiun zone together with experimental data. Along the line $\bar{\Gamma} - \bar{H}$, one may observe a very good agreement between experiment and theory (Fig. 12(a)). If the momentum transfer is changed, so that one goes outside the first Brillouin zone, the different spin wave branches can be determined. This is analysed in detail in Section 4.1. In Fig. 12(b) we show the obtained magnon dispersion, where the optical modes can be clearly observed.

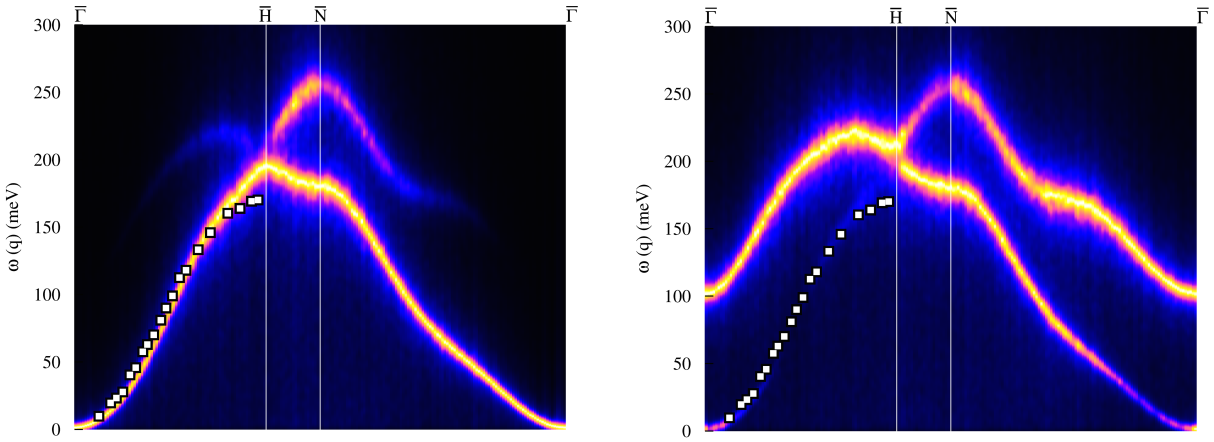

Figure 12: (Color online) Spin wave dispersion spectra obtained from ASD simulations of 2 ML Fe/W(110) at T=300 K and $\alpha = 0.01$. (a) Sampling inside the first Brilloiun zone ($\boldsymbol{\tau} = [00]$) (b) Sampling shifted by vector $\boldsymbol{\tau} = [10]$. Experimental values obtained by SPEELS are marked by white squares [73].

As we mentioned in Sec. 4.1, making use of Eq. 8 in order to describe the susceptibilities as in neutron scattering theory [61], we can probe the magnetic excitations outside the first Brillouin zone.

Given a reciprocal vector $\boldsymbol{q}$ within the primitive Brillouin zone (BZ), we probe the magnon spectrum within the first BZ, as we show in Fig 12(a). Now let's consider $\boldsymbol{\tau} = [hkl] = h\boldsymbol{b}_1 +$

$k\boldsymbol{b}_2 + l\boldsymbol{b}_3$. By changing the momentum transfer by varying $\boldsymbol{\tau}$, we can now probe outside the first BZ. In this way, the intensity of the acoustic and optical branches is changing (Fig. 12(b)).

We now analyse the data in Fig 12, using the discussion around Eq. 8 the case of the Fe bilayer on W(110), $\boldsymbol{\tau} = [0\ \frac{1}{\sqrt{2}}\ 0.5]a$ and the reciprocal vectors are restricted in the film-plane (l=0), then it follows that $\boldsymbol{\phi} = h\pi + k\pi$. Inside the primitive BZ, the phase $\phi = 0$ and in the limit $\boldsymbol{q} \to \boldsymbol{0}$, in Eq. (8) the acoustic term will dominate and will be detected in experiment. If we go outside the first BZ, it is possible to have a situation where the optical term dominates, on the expense of the acoustic response, for instance by choosing $\boldsymbol{\tau} = [10]$, as illustrated in Fig. 9(b).

Relativistic effects

Udvardi and Szunyogh [75] predicted an asymmetry in the magnon spectrum arising from the Dzyaloshinskii-Moriya interaction. Later on it was experimentally detected by Zakeri *et al.* [76] in a Fe bilayer on W(110). The spin wave asymmetry ΔE is defined as the difference in the spin wave energy $\omega(\mathbf{q})$ between $\mathbf{q}$ and $-\mathbf{q}$, i.e $\Delta E = \omega(\mathbf{q}) - \omega(-\mathbf{q})$. If Dzyaloshinskii-Moriya interactions are absent, i.e. very weak effect from spin-orbit interaction, the asymmetry is zero for every wave vector $\mathbf{q}$. In Fig. 10, we show our calculated spin wave asymmetry for the Fe bilayer on W(110) for wave vectors ranging from $-\bar{H}$ to $\bar{H}$ in the two dimensional Brillouin zone, using theoretically determined Dzyaloshinskii-Moriya interaction parameters

The simulations were performed at room temperature, as in experiment, with realistic damping. We obtain a qualitatively good agreement with experiment but the amplitude of the calculated spin wave asymmetry is slightly overestimated ($\approx 12meV$ compared to $\approx 8meV$ in experiment). There are several explanations to this discrepency, primarily the asymmetry is sensitive to the value of the Dzyaloshinskii-Moriya interaction which is very delicate to calculate from ab-initio theory. The assumption made in the calculations of an atomically sharp interface between Fe and W may also be a limiting factor.

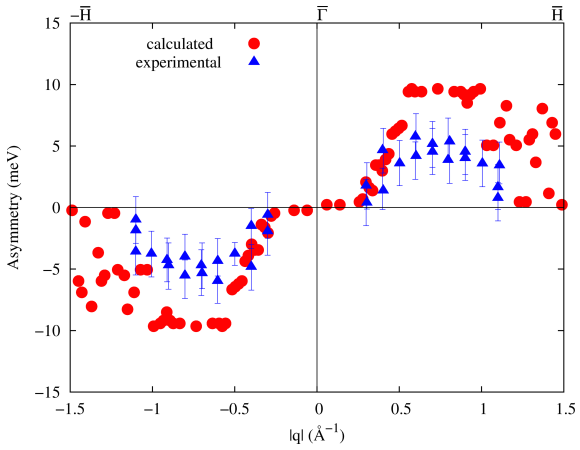

Figure 13: (Color online) Calculated spin wave asymmetry for the magnon spectrum of 2 ML Fe/W(110), using theoretically determined Dzyaloshinskii-Moriya interactions. The experimental values have been obtained by Zakeri et al. [76] for M ∥ [$\bar{1}$10].

4.3.2 Fe on Cu(001)

The Fe multilayers on a Cu(001) substrate represent a rather complex system, since Fe doesn't naturally exist in the fcc phase at low temperatures, thus making it difficult to grow thicker layers of Fe with good quality. It is also well known, from theory, that bulk fcc Fe exhibits a complicated magnetic phase diagram with many magnetic configurations with similar energies. The same thing is true for thick Fe layers on Cu. However, for thin Fe layers (1 to 3 ML), it is generally accepted that Fe adopts a ferromagnetic configuration. In the case of thicker layers there are several proposed magnetic configurations, for instance Sandratskii[77] proposed that the magnetic structure takes the form $\downarrow\uparrow\uparrow$ for the three upper layers. We performed Monte Carlo simulations using calculated exchange parameters starting from either a ferromagnetic configuration or the proposed magnetic structure of Sandratskii as reference state for the 3 ML case. Regardless of the starting configuration, we always obtained the ferromagnetic alignment as the ground state magnetic configuration for 3 ML Fe on Cu001. However, the spin waves (Fig. 14) are soft which is reflected in the calculated adiabatic spin wave stiffness constant D = 210 meV Å^2, which is lower than what we obtain for 1 ML of Fe on Cu001, namely D= 260 meV Å^2. We would like to point out that the ASD method gives a more realistic description of the magnon spectra (Fig 14) than the adiabatic approximation (Fig. 5(b)).

The spectra of 3 ML Fe/Cu(001) presented in Fig. 14 present rather soft magnon curves. The optical branch for the Fe system is more pronounced at low temperatures but it is suppressed close to the $\bar{\Gamma}$-point for reciprocal vectors inside the Brillouin zone. For realistic conditions, i.e. at room temperature and for larger damping, the intensity of the optical branches is very weak and smeared traces of those branches remains visible mostly in the $\overline{\mathrm{X}} - \overline{\mathrm{M}}$ region. As we mentioned before, it is very difficult to grow thick layers of fcc Fe on a Cu substrate and as a consequence there are no experimental data available for this system.

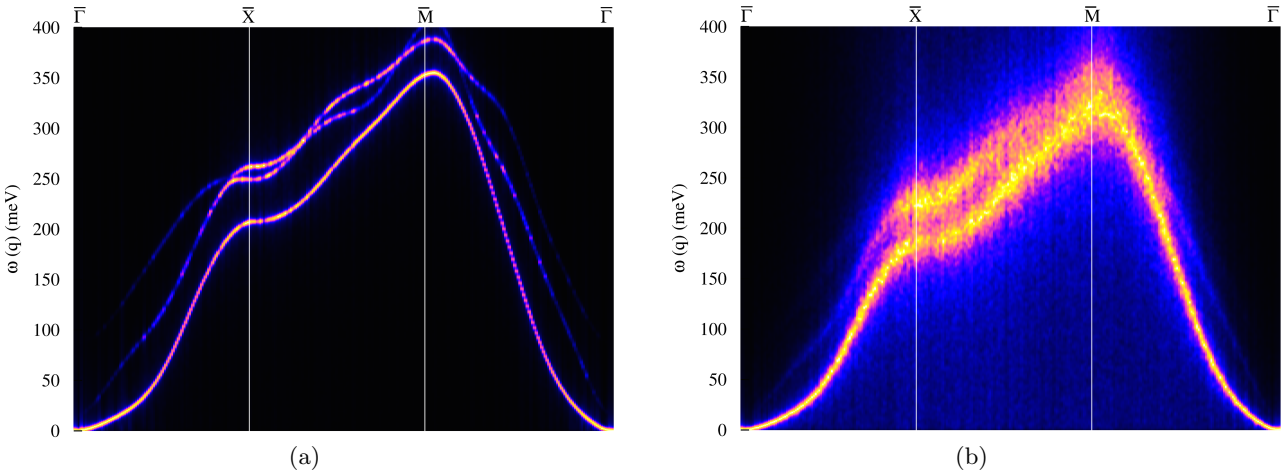

Figure 14: (Color online) Spin wave dispersion spectra obtained from ASD simulations of 3 ML Fe/Cu(001) at (a) T= 1K and small damping constant $\alpha = 3 \times 10^{-4}$ and (b) T = 300 K and realistic damping constant $\alpha = 0.05$

4.3.3 Fe on Ir(001)

In a recent paper[9] Zakeri and coworkers provide experimental data of collective magnetic excitations of thin film systems, among which also 6 layers of Fe on Ir(001). In this experimental study, SPEELS method was used to map out magnon energies. The mentioned experimental results (Fig.3 in the work of Ref.[9]) show only one mode which is detected with reasonably high intensity. We reproduced the experimental data representing the acoustic branch (yellow circles) in Fig. 15 and compared it to the UppASD simulated magnon spectrum.

We point out that all the optical modes (as well as the acoustic mode) calculated by first principles theory, or as obtained from a Heisenberg Hamiltonian, for multilayer magnetic systems, are indeed allowed excitations. In Fig. 6 presented above, we show the adiabatic magnon spectrum for 6 ML Fe/Ir(001) and obviously all modes appear with equal probability and intensity. From the ASD results (Fig. 15), it is clear that the acoustic mode has the highest intensity and is clearly visible if scattering processes with momentum transfer within the first Brillouin zone are considered. The energies and wave vector transfers probed in experiment are: energy loss up to 150 meV and $\Delta K_{\parallel}$ between 0.5 and 0.8 $Å^{-1}$, for both $\bar{\Gamma}$-$\bar{X}$ and $\bar{\Gamma}$-$\bar{M}$ (Fig. 2e,f in Ref. [9]), even up to 250 meV energy loss at the $\bar{X}$-point (Fig. 3b in Ref. [9]). For these energy and wave-vector transfer ranges, the first and second low-energy modes should be observed in experiment, if the data in Fig. 6 were to be used without further processing.

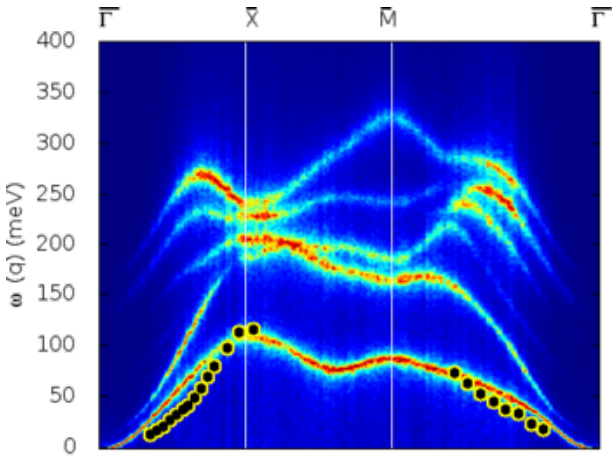

Figure 15: Simulated spin-wave excitation spectra for 6 Fe layers on Ir(001) at 300K. The experimental points represent recently published SPEELS data [9] measured at room temperature.

The structural parameters used in this calculation were the same as reported in Ref.[9]. We considered Heisenberg exchange, using the expression of Ref. [11] as implemented in Ref. [37]. The spin-dynamics simulations were performed at the same temperature as the experimental data of Ref. [9], i.e. 300 K. From Fig. 15 it is clear that the measured acoustic branch reported in the SPEELS experiment is reproduced by theory. It is also clear that all optical branches along $\bar{\Gamma}$-$\bar{X}$ and $\bar{\Gamma}$-$\bar{M}$ directions have either very weak intensity or are vanishing altogether, which explains their absence in the measurements. Fig. 15 also shows that it is possible that a very weak signal from the first optical branch could be detected in experimental investigations, at least if momentum transfers not too close to the zone-center are considered. The first optical

mode along the $\bar{M}$-$\bar{X}$ direction should be detectable, although Stoner excitations may play a role in this case.

Our simulations show the vanishing optical modes in the first Brillouin zone. This is in agreement with what it is observed also in neutron scattering experiments [61], where the optical modes are detected only in the extended zone, and previous spin dynamics studies on thin films [10, 16, 17].

4.3.4 Co on Cu(001)

The fcc Co/Cu(001) system represents a model system for the study of magnetic phenomena in thin films, since it does not exhibit strong structural, chemical or magnetic instabilities. [78, 79] It was therefore a natural candidate for investigation with SPEELS, and became the first ultrathin system in which its magnon spectrum was measured using this method. [41] The system could be described to a good level of accuracy within the context of the nearest-neighbour Heisenberg model on a semi-infinite substrate. In this case a surface mode exists with a dispersion curve $\hbar\omega^{(\mathrm{surf})} = 8JS(1 - \cos(qa_0))$ along the $\langle 110 \rangle$ direction, where J is the exchange coupling, S is the magnitude of the spin per primitive unit cell, q is the length of the magnon wave vector and $a_0 = 2.55$ Å. The fit of this curve to the measured SPEELS data gave $JS = 15.0 \pm 0.1$ meV, which compares well with the value of $JS = 14.7 \pm 1.5$ meV obtained from neutron data of bulk fcc Co at long wave lengths [80] (*i.e.* in the regime $q < 0.3$ Å^{-1}).

The Halle group followed up their initial report for the 8 ML film [41] with results relevant to Co/Cu(001) systems with decreasing thickness down to 2.5 ML. [81, 82] These experiments demonstrated a very weak reduction in the energies required to excite the spin waves, relative to the bulk. [80] However, for all the thicknesses reported, the surface mode at the surface Brillouin zone boundary (the $\overline{\mathrm{X}}$ point) is well below the bulk band edge, at around 240 meV. This difference is for the most part caused by the reduced number of nearest neighbours (NN) at the surface (only 8 atoms) with respect to the bulk case, where there are 12 NN present. [41] For energy ranges where Stoner excitations are important, no direct comparison between calculated and experimental data for bulk Co is possible at the moment.

Theoretical investigations of Co/Cu(001) thin films have been carried out using both the adiabatic approximation [38, 42] and the random phase approximation (RPA) to a description of the spin response of the itinerant electron system. [28, 29]

As explained above, the adiabatic approximation becomes questionable at higher energies and/or large wave-vecors, since Stoner excitations become relevant. In order to address this issue, Costa *et al.* [28, 29] have developed a theory that explicitly takes these excitations into account. Their approach successfully describes the SPEELS measurements for the 8 ML Co/Cu(001) system: their calculated magnon spectrum is in agreement with the experiment over all the $\overline{\Gamma} - \overline{\mathrm{X}}$ line and correctly predicts a broadening of the "acoustic" spin wave peaks, along with an absence of standing spin waves giving rise to "optical" branches. Their work strongly indicates that the process known as Landau damping, through which the spin waves decay into the Stoner continuum, is at play in the Co/Cu(001) system.

At present, the UppASD method cannot handle one-particle Stoner excitations (these are responsible for the longitudinal fluctuations of the magnetic moments) on equal footing with the

transversal fluctuations, although recently efforts have been made to include these effects in the LLG-equation, both directly[83] and indirectly[84]. However, the UppASD method allows to address an alternative source of damping, namely due to the temperature, and we have performed simulations for different thicknesses of Co overlayers (1, 2, 3, 5 and 8 atomic layers) under two very different conditions (Figs. 16, 17, 18 and 20). First we performed simulations at low temperature (1 K), where the damping constant α in Eq. (3) is set to 3×10^{-4}, a value that ensures a very weak coupling to the temperature bath. In this case the temperature effects are deliberately kept to low. In addition, we perform simulations in more realistic conditions, namely at room temperature (T=300 K) and a physically more plausible damping constant $\alpha = 0.05$. For the case of 1 ML on Cu(001) and Cu(111) since the critical temperature of 1 ML Co/Cu(111) is estimated at 255 K and lays below the room temperature, the simulations for both systems were performed at T= 200 K. In this way we make sure that the simulation conditions are below the Curie temperature. All these results are discussed in detail in the following sections.

2 and 3 ML Co/Cu(001)

Qualitatively, the 2 ML and 3 ML case are not so different so we only display the calculated dynamic structure factor for 2 ML Co in Fig. 16. Having more than one layer on top of Cu(001),

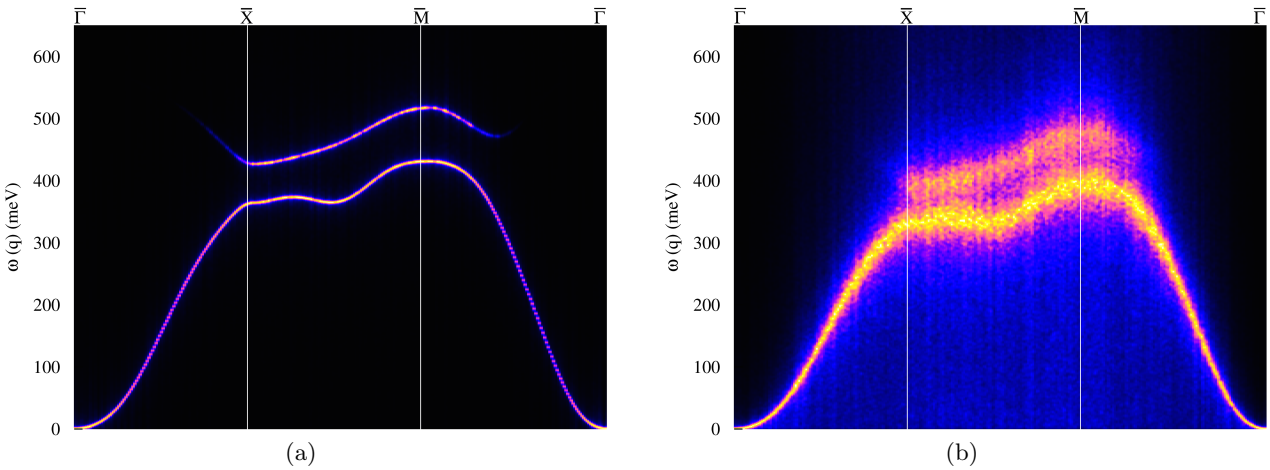

Figure 16: (Color online) Spin wave dispersion spectra obtained from ASD simulations of 2 ML Co/Cu(001) at (a) T= 1K and small damping constant $\alpha = 3 \times 10^{-4}$ and (b) T = 300 K and realistic damping constant $\alpha = 0.05$

we expect, apart from the acoustic branch also optical branches to appear in the magnon spectra, similar to what is found in the adiabatic spectra. In the case of 2 ML we expect one branch of each kind, but as noticed in Fig. 16(a), even at very low temperature (T= 1 K) and extremely small damping, the optical branch is very weak, especially at small wave vectors, close to the $\overline{\Gamma}$-point. The reason for this has been discussed above and it is not pursued further here. Moreover, we note in Fig. 16 that eventhough the microscopical interactions used in the Hamiltonian are the same, for both Figs. 16(a) and 16(b), the spin-wave excitation spectra are different. Not only has the finite temperature the effect of broadening the magnon dispersion curves, in addition there is a shift in the excitation energies themselves (this can be better seen in Fig. 17). This is

due to the fact that Fig. 16 represents data from a dynamical object, which is naturally different when estimated at different temperatures. We exemplify a similar case for another system, this time containing 5 layers of Co on a Cu(001) substrate (Fig. 18).

The spectra of Co layers on Cu(001) are rather different from what we have seen in the previous Sec. 4.3.2 for Fe layers on Cu(001). The fcc Fe/Cu001 system is more complex than the Co/Cu001, as we discussed before. Since fcc Co exists in a wide range of temperatures, it can be grown without problems in very thin (1ML) or thick layers. Comparing the spectra of Fe/Cu(001) presented in Sec. 4.3.2, Fig. 14 to the Co/Cu001 magnon spectra, we notice that they are quite different, with the most striking feature being the overall stiffness of the Co magnon curves with respect to Fe. However, we should keep in mind that the critical temperature for the 3 ML Fe/Cu(001) is much lower than for the analogous Co system. Similar to what we have observed in the case of Fe/Cu001, the optical branch of the Co systems is suppressed close to the zone centre (near the $\bar{\Gamma}$-point, for reciprocal vectors laying within the first Brillouin zone). When increasing the temperature in the simulation, the magnon curves become smeared and broadened, with the optical branches being the most affected by the change in temperature.

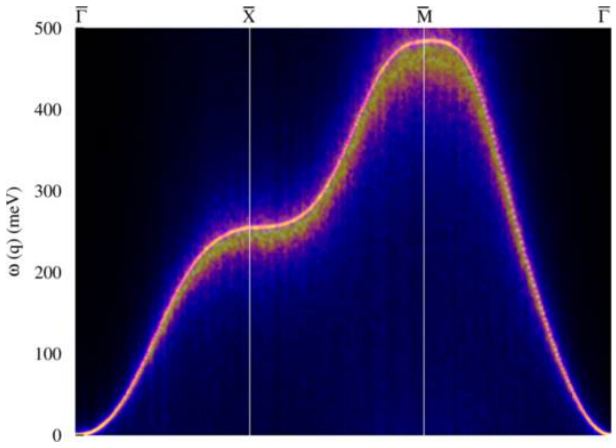

Figure 17: Simulated spin-wave excitation spectra for 1 layer of Co on a Cu(001) substrate. The thin light line represents the magnon dispersion curve simulated at a low temperature of T=1 K, while the softer and broader (smeared) curve represents the magnon excitation estimated at T= 300K.

8 ML Co/Cu(001)

Recently effort is being made for the experimental determination of the layer-resolved exchange coupling. Theoretical studies are able to predict the size and type of inter- and intra-layer exchange coupling in almost any type of systems. In a very recent work [85], the EELS technique has been used to probe Co layers of different thincknesses (from 4 to 8 layers) deposited on a Cu(001) substrate. Rajeswari et al. [85] compared the measured dispersion curves of the so-called 'surface' and 'standing' modes with calculated values [29, 17]. The initial idea was to develop an experimental method that could probe the layer-resolved exchange coupling, but this remains a challenge for the experimental groups. The main achievement resulted from the comparison between the measured and calculated dispersion curves, resides in the possibility

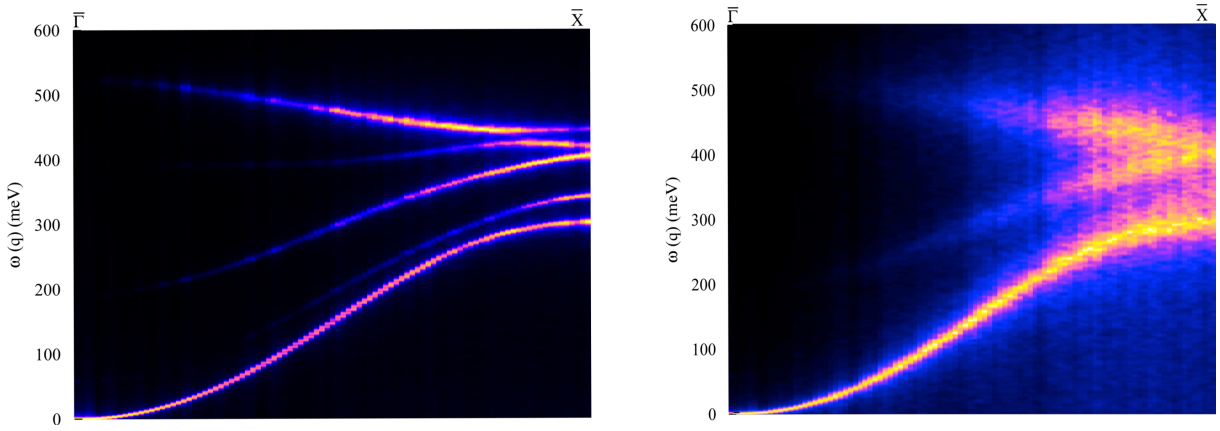

Figure 18: Simulated magnon dispersion spectra for 5 ML Co/Cu(001) at 300 K with two different damping parameter values: α= 0.0003 and 0.05. The stochastic field that simulates the presence of thermal fluctuations in the system is influenced both by the temperature and the damping parameter.

of benchmarking the existent theoretical models used to calculate the exchange interactions and simulate the magnon spectra. The EELS data have been compared with three different theoretical methods: (i) the strategy employed by Costa et al. [29], (ii) the approach described in this review [17] and (iii) a less realistic model of a nearest-neighbour Heisenberg model, with constant exchange coupling constant. We reprinted Fig.3 from Ref [85] (see Fig. 19).

The main conclusion from the experimental study of Rajeswari et al. [85] is that the best fit to the experimental data is provided by the less realistic nearest neighbour Heisenberg model with a constant exchange parameter of 15 meV, since there is no metal known to have only significant nearest neighbour exchange interaction. The experiments are equally well reproduced by the first principles calculated layer-resolved exchange parameters [17], scaled to 85% of their value. Clearly a nearest neighbour model is not a realistic description, especially for metals. Also the necessity of downscaling the calculated exchange interactions by 15% in order to give a very good fit of the measured data, is most likely due to the fact that we evaluated the exchange parameters for a collinear configuration, instead of the disordered non-collinear finite temperature configuration. It has been recently proven that the latter gives weaker exchange interactions. [20] We expect that, in addition, by going beyond the 'rigid-spin' approximation and by including longitudinal fluctuations in our calculations, the values of the exchange parameters will be further decreased leading to softer dispersion curves and consequently a better agreement with the experimental data.

Fig. 20 displays the spin wave spectra on the full 8 ML Co stack on Cu(001), as obtained from the spin-dynamics simulations. It is immediately noticed that the contrast between the calculated spectrum based on the dynamical structure factor (Fig. 20(a)) with the spectrum directly obtained from first-principles (Fig. 5(a)) is strong for values of q close to the $\bar{\Gamma}$-point. In Fig. 20, there is little trace of the 'optical' branches even in the case of low temperature and damping. We also note that at 300 K, the magnon energies at the zone boundaries are reduced by roughly 25 meV, similar to the 2 ML case. The suppression of optical branches arising from

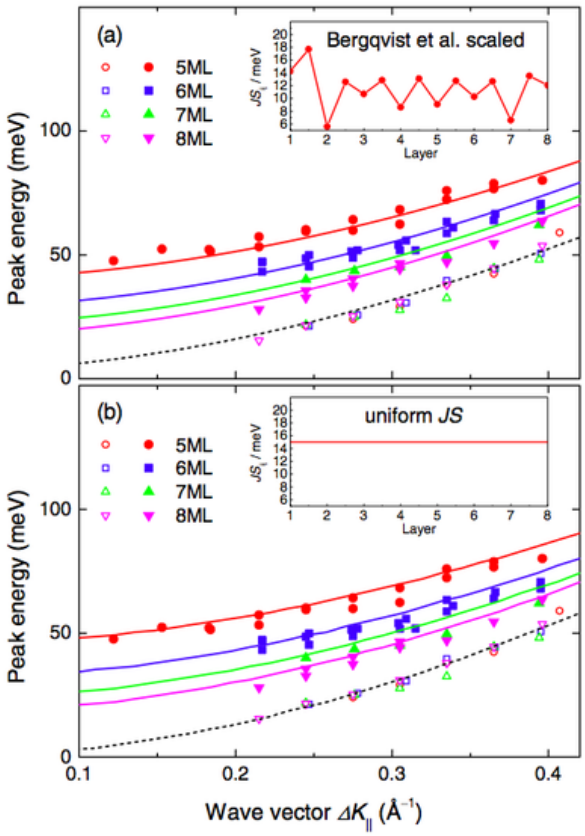

Figure 19: Co multilayers (5, 6, 7 and 8) on Cu(001) substrate. The empty symbols represent the dispersion of the so-called 'surface mode', while the filled symbols represent the dispersion of the so-called 'standing mode'. (a) The solid and dashed lines represent the standing and surface modes estimated from the calculated exchange parameters from Bergqvist et al. [17]. (b) The solid and dashed lines represent fits to the experimental data made by the simple nearest-neighbour Heisenberg model, with a constant exchange parameter. The insets display the exchange parameters values used for the fitting: (a) Bergqvist et al. [17] and (b) constant exchange of JS=15 meV. (We reproduced here Fig. 3 from Rajeswari et al. [85]

a dynamical treatment has also been pointed out by Costa *et al.* [28, 29]. We also note that the agreement between the theoretical acoustic branch that we calculated and experiment is rather good.

1 ML Co/Cu(001) vs. Co/Cu(111)
Magnon spectra for different surface orientations

Fig. 21 displays the spin wave spectra in a 1 ML thick Co layer on Cu(001). The values of the exchange parameters In the low temperature case (Fig. 21(a)), the spectra obtained from the atomistic spin dynamics simulations is almost indistinguishable from the adiabatic spectra. We point out that these results are obtained from a calculation of the dynamical structure factor $S(\mathbf{q}, \omega)$. In order to facilitate the comparison between the spin wave spectra for a single layer of Co on Cu for different orientations of the substrate, we performed the calculations for

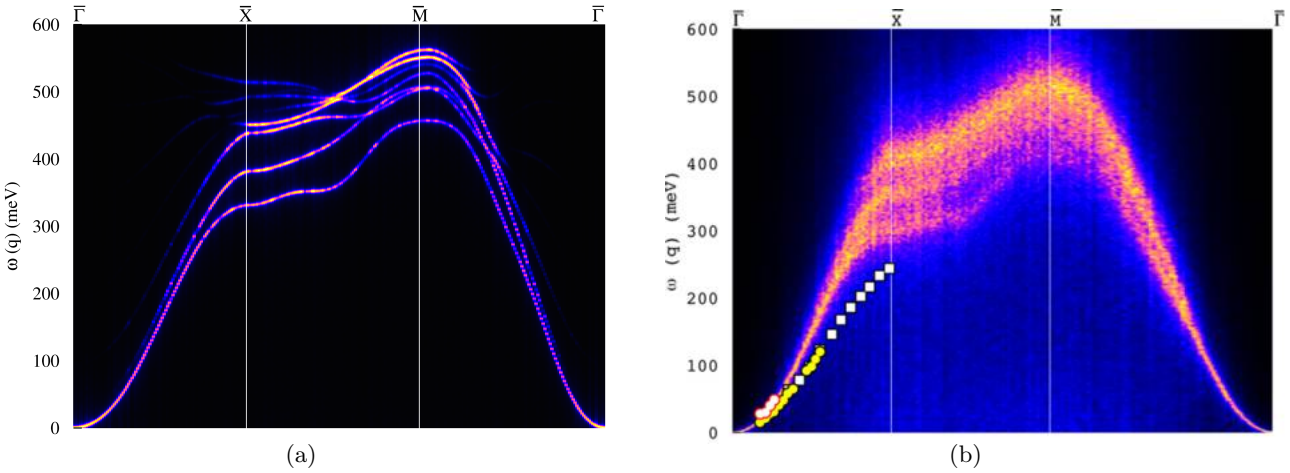

Figure 20: (Color online) Spin wave dispersion spectra obtained from ASD simulations of 8 ML Co/Cu(001) at (a) T= 1K and small damping constant $\alpha = 3 \times 10^{-4}$ and (b) T = 300 K and realistic damping constant $\alpha = 0.05$. Experimental values obtained by SPEELS are marked by white squares [41], while data measured by EELS is marked by yellow circles and red circles [86] representing the first optical branch.

both Cu(001) and Cu(111) orientations (discussed in detailed below), at the same value of the temperature, i.e. T= 200 K. Increasing the temperature and damping (Fig. 21(b)) causes some broadening of the dynamical structure factor and as a result the magnon energy at the BZ boundary ($\overline{\text{X}}$ and $\overline{\text{M}}$ points) decreases slightly. However, overall the effects of temperature and dynamic treatment are not significant in this case.

Fig. 21 shows primarily that the surface magnons depend critically on the orientation of the substrate, since for the [111] oriented substrate, the magnon dispersion is softer then for the [001] oriented surface. This reflects the combination of the geometry and the range and nature of the Heisenberg exchange interactions. The main difference resides in the geometry of the system: the close-packed nature of the [111] surface with respect to the open-structure character of the [001]. This leads to stronger nearest neighbour exchange interactions (1.89 mRyd) for the [001] orientation and consequently stiffer spin-wave dispersion spectrum than in the case of the [111] orientation, characterised by much weaker exchange (1.06 mRyd) and a softer magnon curve. This can be noticed from the data presented in Fig. 21.

5 Conclusions and Outlook

In this review we have outlined some of the details about atomistic spin-dynamics simulations and how such simulations can be coupled to first principles theory for the electronic structure, in order to calculate magnetic moments and relevant magnetic parameters (exchange interaction, Dzyakloshinskii-Moryia interaction and magnetic anisotropy). The atomistic description of magnetisation dynamics has several appealing aspects as compared to micromagnetic simulations. Firstly it identifies a correct smallest unit to consider as a dynamical object, i.e. the atomic spin. This is an obvious advantage since it connects to the building block of a material, the atom. In addition, this approach has no problems with considering antiferromagnetic,

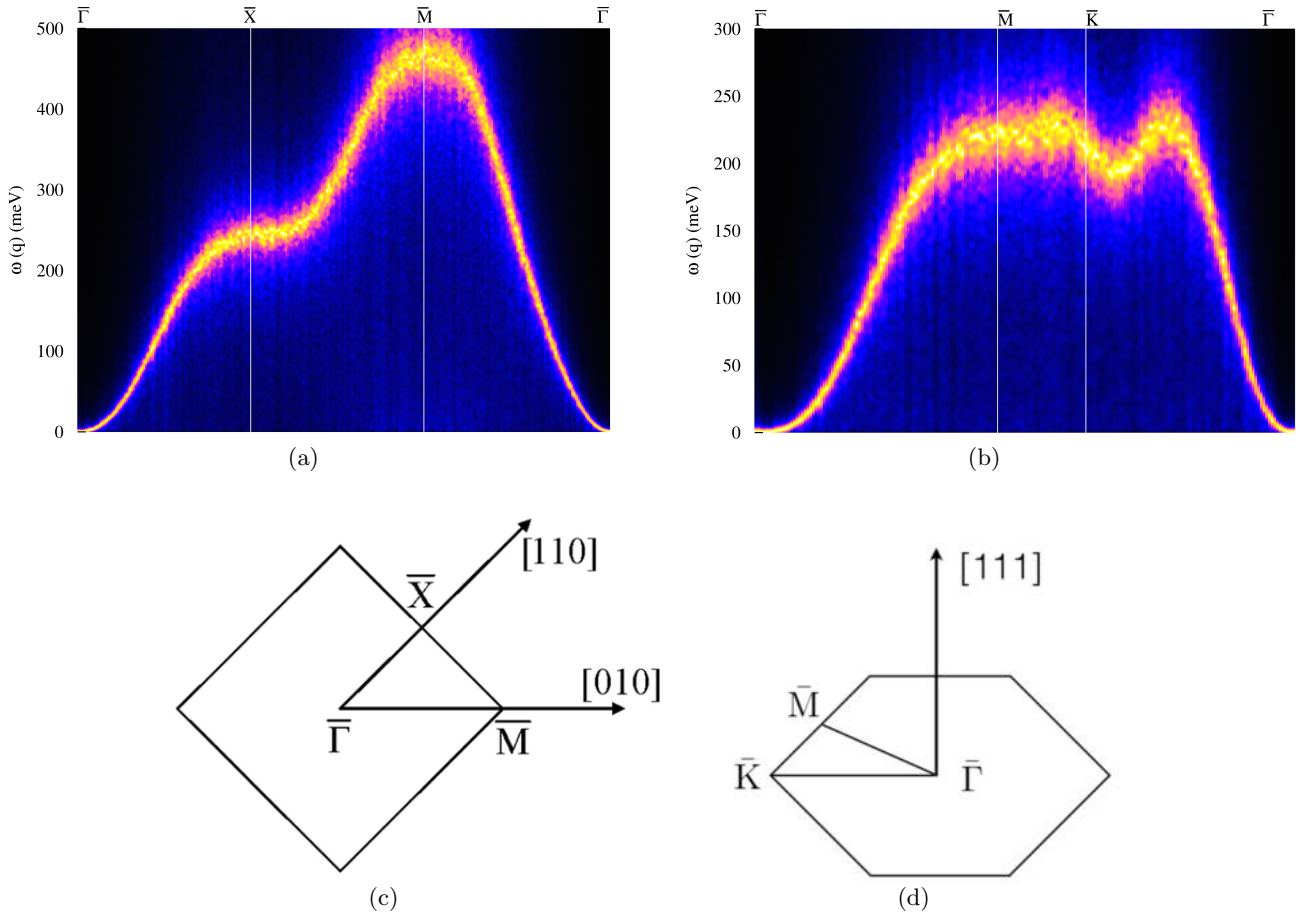

Figure 21: (Color online) Spin wave dispersion spectra obtained from ASD simulations of (a) 1 layer of Co/Cu(001) and (b) 1 layer of Co/Cu(111), both at T= 200 K and realistic damping constant $\alpha = 0.05$. The corresponding Brillouin zones for the 001-orientation (c) and for the 111-orientation (d).

ferromagnetic or ferrimagnetic materials, which is also an advantage, and it allows also for on the fly evaluation of the relevant parameters used in the simulation, so that their temperature dependence may correctly be incorporated. In this review we have focused primarily on how this multi-scale technique can be used for calculating magnon dispersion relationships, for both bulk and surfaces, although it can in principle be applied to a wide range of problems connected to magnetisation dynamics. Here, we have made a comparison between theoretical magnon dispersions for one to a few layers of Fe and Co on different substrates, such as W (110), Cu (001) and Cu(111). In general, the agreement between observations and theory is good, e.g. the measured acoustic modes of the surface systems are in general softer compared to bulk magnons, which is reproduced by theory. In addition, the optical modes, although being allowed excitations in principle, are not visible or only weakly visible in the experiments, a fact which is captured by theory. This is explained here, as well as in Ref. [10], by focusing on the scattering nature of the SPEELS experiments, where the differential cross section and hence dynamical structure function are relevant quantities. Thus it is argued here that a natural way to understand SPEELS experiments is to consider time and space displaced spin-correlations, as manifested in the dynamical structure function $S(q, \omega)$. A further development of this theory

for SPEELS is to consider that the penetration depth of electrons in this experiment is not as long-ranged as e.g. for neutrons in a corresponding neutron scattering experiment, and to consider Stoner excitations which become relevant for larger values of the momentum transfer. Elevated temperatures have in the current implementation of atomistic spin-dynamics the effect of softening shifting and broadening the magnon excitation spectrum, even though the exchange parameters are calculated at zero temperature. This is due to that $S(q, \omega)$ samples, via the spin-correlations, a true dynamical object. This is different from a static approximation, as is done when adopting the adiabatic magnon approximation, as outlined in Section 3.3 in this review. In some cases finite temperatures can modify the magnon frequency with up to 15%, depending on system [17]. A further development for these thin film systems is to include also temperature dependent exchange interactions, as was done in Ref. [20] for bulk bcc Fe, and possibly be also to consider the temperature dependence of the Dzyakloshinskii-Moryia interaction. In this way most of the relevant temperature effects are included in the simulations.

Our ambition is to further develop the methods that we currently use by extending even more their range of applicability. We are already working on finding a better way of treating complex (non-collinear) magnetic structures and their properties from *ab initio*, allowing longitudinal fluctuations of magnetic moments in ASD, giving an estimate of the magnon lifetimes (which is already probed experimentally) and trying to find a reliable way for calculating the damping parameter α. An improved implementation of dipolar interactions based on Fast Multipole Method (FMM) in the UppASD is almost ready. This will allow us to investigate also dipolar magnons, besides the exchange magnons. This comes in addition to the massive parallelisation already implemented for UppASD, as described before. Another development of the method described here is to couple spin- and lattice-dynamics. This is far from a trivial task since the time-scales are similar. It should be noted that already in the original article that derive the atomistic spin-dynamics equations [12], a suggestion for how to couple spin- and lattice-dynamics was made. The most efficient numerical scheme for performing this has most likely not been found yet. However, given the experimental interest in these coupled dynamical objects, e.g. the dynamics of multiferroic materials, such a development is highly interesting.

Finally, we mention that further challenges both for theory and experiments is to consider new geometries and new surface systems, e.g. magnetic clusters or molecular magnets [87] that may be exchange coupled to a substrate [88]. An analysis of the magnetisation dynamics of such systems is highly challenging both from an experimental and theoretical point of view, in particular since the dynamics of molecular magnets most likely requires a quantum description, and one would have to incorporate this part with the classical description of atomistic spin-dynamics approach. A further direction of research for SPEELS experiments as well as atomistic spin-dynamics simulations is the emerging field of magnonics, where the generation and detection of magnetic excitations, e.g. magnons, skyrmions and merons, is of crucial importance. This field is however, outside the scope of the current review.

Acknowledgement

We gratefully acknowledge Lars Nordström, Johan Hellsvik and Björn Skubic for their work on the ASD method used in this highlight. Hubert Ebert is acknowledged for providing the SPR-KKR software package. The European Research Council (ERC), the Swedish Research Council (VR), the Knut and Alice Wallenberg (KAW) Foundation, Carl Tryggers Foundation and Göran Gustafsson Foundation are acknowledged for financial support. O.E. and A.B. acknowledge eSSENCE and L.B. acknowledge SeRC. The computer simulations were performed on resources provided by the Swedish National Infrastructure for Computing (SNIC) at National Supercomputer Centre (NSC), UppMAX, PDC and High Performance Computing Center North (HPC2N).

References

[1] C. Kittel, "Introduction to Solid State Physics".

[2] G. L. Squires, "Introduction to the theory of thermal neutron scattering".

[3] J. Stöhr and H. C Siegmann, "Magnetism: from fundamentals to nanoscale dynamics".

[4] A. Zangwill, "Physics at Surfaces".

[5] J. Kübler, "Theory of Itinerant Electron Magnetism".

[6] M. Plihal, D. L. Mills, and J. Kirschner. *Phys. Rev. Lett.*, 82:2579, 1999.

[7] J. Prokop, W. X. Tang, Y. Zhang, I. Tudosa, T. R. F. Peixoto, K. Zakeri, and J. Kirschner. *Phys. Rev. Lett.*, 102:177206, 2009.

[8] A. T. Costa, R. B. Muniz, J. X. Cao, R. Q. Wu, and D. L. Mills. *Phys. Rev. B*, 78:054439, 2008.

[9] Kh. Zakeri, T.-H. Chuang, A. Ernst, L. M. Sandratskii, P. Buczek, H. J. Qin, Y. Zhang, and J. Kirschner. *Nature Nanotechnology*, 8:853, 2013.

[10] A. Taroni, A. Bergman, L. Bergqvist, J. Hellsvik, and O. Eriksson. *Phys. Rev. Lett.*, 107:037202, 2011.

[11] A. I. Liechtenstein, M. I. Katsnelson, and V. A. Gubanov. *J. Phys. F: Metal Phys.*, 14:L125, 1984.

[12] V. P. Antropov, M. I. Katsnelson, B. N. Harmon, M. van Schilfgaarde, and D. Kusnezov. *Phys. Rev. B*, 54:1019, 1996.

[13] V. P. Antropov, M. I. Katsnelson, M. van Schilfgaarde, and B. N. Harmon. *Phys. Rev. Lett.*, 75:729, 1995.

[14] B. Skubic, J. Hellsvik, L. Nordström, and O. Eriksson. *J. Phys. Condens. Matter*, 20:315203, 2008.

[15] U. Nowak, O. N. Mryasov, R. Wieser, K. Guslienko, and R. W. Chantrell. *Phys. Rev. B*, 72:172410, 2005.

[16] A. Bergman, A. Taroni, L. Bergqvist, J. Hellsvik, B. Hjörvarsson, and O. Eriksson. *Phys. Rev. B*, 81:144416, 2010.

[17] L. Bergqvist, A. Taroni, A. Bergman, C. Etz, and O. Eriksson. *Phys. Rev. B*, 87:144401, 2013.

[18] J. H. Mentink, J. Hellsvik, D. Afanas, B. A. Ivanov, A. Kirilyuk, A. V. Kimel, Olle Eriksson, M. I. Katsnelson, and Th. Rasing. *Phys. Rev. Lett.*, 108:057202, 2012.

[19] J. Chico, C. Etz, L. Bergqvist, J. Fransson, A. Delin, O. Eriksson and A. Bergman, arXiv:1308.0986 (2013).

[20] A. Szilva, M. Costa, A. Bergman, L. Szunyogh, L. Nordström, and O. Eriksson. *Phys. Rev. Lett.*, 111:127204, 2013.

[21] J. M. D. Coey, "Magnetism and Magnetic Materials", Cambridge University Press 2010.

[22] Luuk J. P. Ament, Michel van Veenendaal, Thomas P. Devereaux, John P. Hill, and Jeroen van den Brink. *Rev. Mod. Phys.*, 83:705, 2011.

[23] W. Schweika "Magnetic Excitations and Scattering Experiments" in "Magnetism goes Nano" Eds. Stefan Blügel, Thomas Bruckel, Claus M. Schneider, Springer Verlag (2005).

[24] L. M. Sandratskii, J. Phys.: Condens. Matter **3**, 8565, (1991).

[25] S. V. Halilov, H. Eschrig, A. Y. Perlov, and P. M. Oppeneer. *Phys. Rev. B*, 58:293, 1998.

[26] J. A. Blackman J. F. Cooke and T. Morgan. *Phys. Rev. Lett.*, 54:718, 1985.

[27] S. Y. Savrasov. *Phys. Rev. Lett.*, 81:2570, 1998.

[28] A. T. Costa, Jr., R. B. Muniz, and D. L. Mills. *Phys. Rev. B*, 69:064413, 2004.

[29] A. T. Costa, Jr., R. B. Muniz, and D. L. Mills. *Phys. Rev. B*, 70:054406, 2004.

[30] P. Mohn, Magnetism in the Solid State, Springer Verlag, 2003.

[31] P. Buczek, A. Ernst, and L. M. Sandratskii. *Phys. Rev. B*, 84:174418, 2011.

[32] E. K. U. Gross and W. Kohn. *Phys. Rev. Lett*, 55:2850, 1985.

[33] G. Kresse and J. Furthmüller. *Comput. Mat. Sci.*, 6:15, 2009.

[34] G. Kresse and D. Joubert. *Phys. Rev. B*, 59:1758, 1999.

[35] Zabloudil, Hammerling, Szunyogh, Weinberger, Electron Scattering in Solid Matter, 2010.

[36] J. Minar H. Ebert, D. Ködderitzsch. *Rep. Prog. Phys.*, 74:096501, 2011.

[37] The Munich SPR-KKR package, version 6.3, H. Ebert et al, http://ebert.cup.uni-muenchen.de/SPRKKR.

[38] L. Udvardi, L. Szunyogh, K. Palotas, and P. Weinberger. *Phys. Rev. B*, 68:104436, 2003.

[39] H. Ebert and S. Mankovsky. *Phys. Rev. B*, 79:045209, 2009.

[40] A. Liechtenstein, M. Katsnelson, V. Antropov, and V. Gubanov. *J. Magn. Magn. Mater.*, 54:965, 1986.

[41] R. Vollmer, M. Etzkorn, P. S. Anil Kumar, H. Ibach, and J. Kirschner. *Phys. Rev. Lett.*, 91:147201, 2003.

[42] M. Pajda, J. Kudrnovsky, I. Turek, V. Drchal, and P. Bruno. *Phys. Rev. Lett.*, 85:5424, 2000.

[43] I. E. Dzyaloshinskii. *Sov. Phys. JETP*, 5:1259, 1957.

[44] T. Moriya. *Phys. Rev.*, 120:91, 1960.

[45] V. Kambersky. *Can. J. Phys.*, 48:2906, 1970.

[46] V. Kambersky. *Czech. J. Phys.*, 26:1366, 1976.

[47] M. Fähnle and D. Steiauf. *Phys. Rev. B*, 73:184427, 2006.

[48] S. Mankovsky, D. Ködderitzsch, G. Woltersdorf, and H. Ebert. *Phys. Rev. B*, 87:014430, 2013.

[49] D. Thonig and J. Henk. *New J. Phys.*, 16:013032, 2014.

[50] N. G. V. Kampen. Elsevier Science Ltd, 2008.

[51] O. Hjortstam, K. Baberschke, J. M. Wills, B. Johansson, and O. Eriksson. *Phys. Rev. B*, 55:15026, 1997.

[52] J. Stöhr. *J. Magn. Magn. Mater.*, 200:470, 1999.

[53] J. H. Mentink, M. V. Tretyakov, A. Fasolino, M. I. Katsnelson, and Th. Rasing. *J. Phys.: Condens. Matter*, 22:176001, 2010.

[54] X. Tao, D. P. Landau, T. C. Schulthess, and G. M. Stocks. *Phys. Rev. Lett.*, 95:087207, 2005.

[55] K. Chen and D. P. Landau Phys. Rev. B **49**, 3266, (1994).

[56] S. W. Lovesey, Theory of Neutron Scattering from Condensed Matter (Oxford University Press, Oxford, 1984).

[57] P. Weinberger "Magnetic anisotropies in nanostructured matter" , Taylor & Francis 2009.

[58] J. Hellsvik, B. Skubic, L. Nordström, and O. Eriksson. *Phys. Rev. B*, 79:184426, 2009.

[59] M. Pajda, J. Kudrnovsky, I. Turek, V. Drchal, and P. Bruno. *Phys. Rev. B*, 64:174402, 2001.

[60] M. W. Stringfellow. *J. Phys. C: Solid State Phys.*, 1:950, 1968.

[61] J. Jensen and A. R. Mackintosh, Rare Earth Magnetism: Structures and Excitations Clarendon Press . Oxford 1991.

[62] F. Lopez-Aguilar and J. Costa-Quintana. *Phys. Stat. Sol. (b)*, 123:219228, 1984.

[63] V. I Anisimov, J. Zaanen, and O. K. Andersen. *Phys. Rev. B*, 44:943, 1991.

[64] A. Jacobsson, B. Sanyal, M. Lezaic, and S. Blügel. *Phys. Rev. B*, 88:134427, 2013.

[65] M. T. Hutchings and E. J. Samuelsen. *Phys. Rev. B*, 6:3447, 1972.

[66] F. Essenberger, S. Sharma, J. K. Dewhurst, C. Bersler, F. Cricchio, L. Nordström, and E. K. U. Gross. *Phys. Rev. B*, 84:174425, 2011.

[67] H. J. Elmers. *Int. J. Mod. Phys. B*, 9:3115, 1995.

[68] H. J. Elmers, J. Hauschild, and U. Gradmann. *Phys. Rev. B*, 54:15224, 1996.

[69] R. B. Muniz and D. L. Mills. *Phys. Rev. B*, 66:174417, 2002.

[70] R. Wu and A. J. Freeman. *Phys. Rev. B*, 45:7532, 1992.

[71] D. Böttcher, A. Ernst, and J. Henk. *J. Magn. Magn. Mater.*, 324:610, 2012.

[72] H. A. Mook and R. M. Nicklow. *Phys. Rev. B*, 7:336, 1973.

[73] W. X. Tang, Y. Zhang, I. Tudosa, J. Prokop, M. Etzkorn, and J. Kirschner. *Phys. Rev. Lett.*, 99:087202, 2007.

[74] Kh. Zakeri, Y. Zhang, T.-H. Chuang, and J. Kirschner. *Phys. Rev. Lett.*, 108:197205, 2012.

[75] L. Udvardi and L. Szunyogh. *Phys. Rev. Lett.*, 102:207204, 2009.

[76] Kh. Zakeri, Y. Zhang, J. Prokop, T.-H. Chuang, N. Sakr, W. X. Tang, and J. Kirschner. *Phys. Rev. Lett.*, 104:137203, 2010.

[77] L. M. Sandratskii. *Phys. Rev. B*, 81:064417, 2010.

[78] U. Gradmann, Handbook of Magnetic Materials (Elsevier, Amsterdam, 1993), Chap. 1.

[79] C. A. F. Vaz, J. A. C. Bland, and G. Lauhoff. *Rep. Prog. Phys.*, 71:056501, 2008.

[80] R. N. Sinclair and B. N. Brockhouse. *Phys. Rev.*, 120:1638, 1960.

[81] M. Etzkorn, P. S. Anil-Kumar, R. Vollmer, H. Ibach, and J. Kirschner. *Surf. Sci.*, 566:241, 2004.

[82] R. Vollmer, M. Etzkorn, P. S. Anil-Kumar, H. Ibach, and J. Kirschner. *J. Appl. Phys.*, 95:7435, 2004.

[83] P.-W. Ma and S. L. Dudarev. *Phys. Rev. B*, 86:054416, 2012.

[84] R. Chimata, A. Bergman, L. Bergqvist, B. Sanyal, and O. Eriksson. *Rev. Lett.*, 109:157201, 2012.

[85] J. Rajeswari, H. Ibach, and C. M. Schneider. *Phys. Rev. Lett.*, 112:127202, 2014.

[86] J. Rajeswari, H. Ibach, C. M. Schneider, A. T. Costa, D. L. R. Santos, and D. L. Mills. *Phys. Rev. B*, 86:165436, 2012.

[87] L. Bogani and W. Wernsdorfer. *Nat. Mater.*, 7:179, 2008.

[88] H. Wende et al. *Nat. Mater.*, 6:516, 2007.